AAV delivery of RNA editing machinery rescues SUDEP and seizure phenotype in a mouse model of Dravet Syndrome

Ellie M. Chilcott[1], Juan F. Antinao Diaz[1], Amanda Almacellas Barbanoj[2], Marc Moore[3], Anna Keegan[1], Zakary Waddington[1], Vicky Fang[1], Stephanie Schorge[4], Gabriele Lignani[2], Simon N Waddington[1] & Rajvinder Karda[1*]

Affiliations

[1] EGA Institute for Women's Health, University College London, 86-96 Chenies Mews, London, WC1E 6HX, UK

[2] Queen Square Institute of Neurology, Queens Square, University College London, London, WC1N 3BG, UK

[3] School of Health and Life Sciences, National Horizon Centre, Teesside University, 38 John Dixon Ln, Darlington, DL1 1HG, UK

[4] Division of Biosciences, Medical Science Building, University College London, London WC1E 6BT

[*]Corresponding author: Dr Rajvinder Karda
Maternal and Fetal Medicine Department
Institute For Women's Health
University College London
86-96 Chenies Mews
WC1E 6HX
London
r.karda@ucl.ac.uk

Key words: Adeno-associate virus, RNA editing, CIRTS (CRISPR-Cas-inspired RNA targeting system), preclinical, Dravet Syndrome

ABSTRACT

Dravet syndrome (DS) is a severe childhood genetic epilepsy, caused by *de novo* heterozygous mutations in *SCN1A*, resulting in a loss-of-function of the voltage-gated sodium ion channel, Nav1.1. Nav1.1 is expressed in the brain, and at a lower level, in the heart. DS manifests in the first year of life. Patients exhibit tonic-clonic seizures, febrile seizures, cognitive decline, developmental delays, ataxia, and sudden unexpected death from epilepsy (SUDEP). We have developed a novel AAV-F mediated CRISPR-Cas-inspired RNA targeting system (CIRTS) preclinical treatment to increase endogenous *Scn1a* and ameliorate the disease phenotype in a clinically-relevant heterozygous loss-of-function mouse model of DS. We designed novel guide RNAs (gRNAs) to target the long non-coding RNA, (or natural antisense transcript) of *Scn1a* to increase the expression of *Scn1a* mRNA in DS mice. We show that intracerebroventricular and intravenous administration of AAV-F-CIRTS-gRNA9 to target the brain and the heart to neonatal $Scn1a^{+/-}$ mice resulted in a significant increase in survival, and a reduction in SUDEP, febrile seizures and seizure duration. These findings provide proof-of-concept evidence that an AAV-F-CIRTS mediated therapy hold promise as a potential treatment for DS.

INTRODUCTION

Dravet syndrome (DS) is a severe childhood genetic epilepsy, with an incidence rate of 1 in 15,400-40,900 live births worldwide*(1, 2)*. The disease typically manifests within the first year of life accompanied by tonic-clonic seizures, febrile and afebrile seizures, episodes of status epilepticus, cognitive impairment, ataxia and unfortunately, ~15% of patients experience sudden unexpected death in epilepsy (SUDEP)*(3–5)*. >90% of patients harbour *de novo* loss-of-function variants in the *SCN1A* gene which encodes an α-subunit of a voltage-gated ion channel, Nav1.1*(6)*. In humans, Nav1.1 expression has been detected in the hippocampus (including the

60 dentate gyrus, CA3, and CA2 regions), layers V and VI of the cortex, the granular and molecular
61 layers, as well as in the deep nuclei and Purkinje cells of the cerebellum*(7)* and the
62 heart. Previous studies have explored altered cardiac function in individuals with DS and in
63 mouse models, suggesting a potential contribution to SUDEP*(8–11)*.

64 Current anti-seizure medications, including valproate, stiripentol, fenfluramine and
65 cannabidiol can reduce the seizure frequency*(12)*, but the disease manifestation continues. Thus,
66 there remains a significant unmet need to establish an effective long-term treatment for DS.

67 Adeno-associated viral (AAV) vectors, specifically AAV9, have been used extensively
68 for many preclinical*(13, 14)* and clinical trials*(15, 16)*. However, the high doses of AAV9
69 required to achieve efficacious peripheral delivery has also caused liver toxicity and thrombotic
70 microangiopathy*(16, 17)*. As such, there is a need to develop novel capsids that enable efficient
71 therapeutic delivery at a lower dose, avoiding immunotoxicity associated with the gene therapy
72 vector. Novel AAV capsids targeting the central nervous system (CNS) have been generated*(18,*
73 *19)*. One example of this is AAV-F, a novel capsid derived from AAV9, which has shown a
74 greater CNS transduction efficiency relative to the parental AAV9 capsid*(18)* and has been used
75 successfully in a preclinical study to treat a severe mitochondrial disorder*(20)*.

76 RNA targeting technologies have emerged as therapeutic, inspired by successes in
77 oligonucleotide based therapies*(21, 22)*. Targeting RNA is advantageous over DNA as it can
78 influence gene expression without permanent alterations to the host genome and modulate
79 protein expression regardless of the specific mutation. Furthermore, DNA and RNA targeting
80 systems such as Cas9 and Cas13 are built from bacterial proteins and have shown to induce an
81 immune response *in vivo(23)*. A new RNA editing technology has been developed to target RNA
82 sequences, referred to as CRISPR-Cas-inspired RNA targeting system (CIRTS)*(24)*. CIRTS is

83 built from human proteins and previous validation studies *in vitro* and *in vivo* have shown the
84 CIRTS system to modulate protein expression by RNA editing *(24–26)*, although until now this
85 has not been used in a therapeutic setting. In this study, we used a CIRTS construct consisting of
86 a ssRNA binding protein (β-defensin 3), RNA hairpin-binding protein (TBP6.7) and effector
87 protein (YTHDF2)*(24)* to down-regulate target RNA expression.

88 Here, we used the AAV-F-mediated CIRTS technology and designed novel guide RNAs
89 (gRNAs) to edit a *Scn1a* specific long non-coding RNA (lncRNA) of the natural antisense
90 transcript (NAT), which normally functions to negatively regulate *Scn1a* expression*(27)*. In
91 doing so, we aimed to 'inhibit the inhibitor', leading to an upregulation of *Scn1a* mRNA (Fig.
92 1A). We screened 21 gRNAs *in vitro* and selected two lead candidate gRNAs (gRNA9 & 21)
93 which significantly increased endogenous *Scn1a* mRNA and shared highest homology to the
94 human lncRNA sequence. We used a clinically-relevant DS heterozygous (*Scn1a*$^{+/-}$) model,
95 which recapitulates much of the human disease, including spontaneous and febrile seizures, and
96 SUDEP*(28, 29)*. We administered our candidates AAV-F-CIRTS-gRNA 9 & 21 vectors to
97 neonatal DS mice via intracerebroventricular (ICV) and intravenous (IV) administration to target
98 the brain and the heart. Candidate AAV-F-CIRTS-gRNA9 resulted in significant increase in
99 survival over 100 days post-injection. In addition, febrile and spontaneous seizure assessment of
100 DS mice injected with AAV-F-CIRTS-gRNA9 showed a significant reduction in seizure severity
101 and seizure duration. Molecular analysis revealed a significant up-regulation of endogenous
102 *Scn1a* mRNA in treated AAV-F-CIRTS-gRNA9 DS mice compared to untreated DS control
103 mice. Our work demonstrates for the first time, a potential AAV-F mediated RNA editing
104 approach to treat patients with DS.

105

106 **RESULTS**

107 **Design and *in vitro* validation of novel gRNAs targeting *Scn1a* lncRNA**

108 We firstly validated the CIRTS machinery and consistent with previous studies*(24)*,
109 AAV-CIRTS-gRNAluc was able to significantly reduce luciferase expression (Fig. S1). We
110 designed 21 novel gRNA sequences (20-30mer) to target the *Scn1a* lncRNA (Fig. 1A) (here
111 referred to as *Scn1anat*), which were cloned into the AAV-CIRTS plasmid (Fig. 1B). We
112 validated our gRNA designs *in vitro*, in differentiated mouse Neuro2a cells and assessed the
113 effects on endogenous *Scn1a* mRNA expression. Transient transfection of AAV-CIRTS-gRNA
114 constructs onto differentiated Neuro2a cells resulted in a significant increase of endogenous
115 *Scn1a* mRNA by 4 out of 21 AAV-CIRTS-gRNA constructs (Fig. 1C). Constructs containing
116 gRNAs 9, 11, 15 and 21 led to average *Scn1a* mRNA fold changes of 1.89 (P=0.0016), 2.15
117 (P=0.0015), 2.12 (P=0.022) and 2.56 (P<0.0001), respectively. gRNAs 9 and 21 were selected
118 for the *in vivo* study as they showed the highest homology to the *SCN1A* lncRNA (*SCN1ANAT*;
119 93.3% and 100%, respectively) (Fig. 1C).

120

121 **AAV-F-mediated RNA editing in DS mice significantly improves survival**

122 In this study we crossed the males from 129Sv-*Scn1a*^{tm1Kea}/Mmjax model*(28, 29)* with
123 wild-type CD1 females to generate F2 129Sv-*Scn1a*^{tm1Kea}/Mmjax x CD1 heterozygote females,
124 which were then bred to wild-type C57BL/6J males to obtain experimental litters (*Scn1a*$^{+/-}$). This
125 enabled a larger litter size. *Scn1a*$^{+/-}$ mice exhibit spontaneous seizures and SUDEP with an
126 overall survival of 38.2% over 100 days of development (Fig. S2A), febrile seizures (Fig. S2D)
127 and a reduction in *Scn1a* gene expression, particularly in the cortex at P50 (P=0.0078; Fig. S2E),

128 consistent with previous studies*(22, 28, 30)*. RNA-seq of *Scn1a*$^{+/+}$ and *Scn1a*$^{+/-}$ cortical tissue at
129 P50 confirmed 140 up- and 41 down-regulated genes (Fig. S3A and B), with significant down-
130 regulation of *Scn1a* (-0.77Log2FC, P=5.85x10^{-6}; Fig. S2C). Molecular function gene ontology
131 (GO) analysis of the differentially expressed genes in *Scn1a*$^{+/-}$ mice reveal up-regulation in terms
132 related to neuropeptide receptor activity, monoatomic ion transport and voltage-gated sodium
133 channel activity (Fig. S3D).

134 Using this DS mouse model, we sought to determine the optimal capsid and gRNA
135 combination by generating AAV-F and AAV9 vectors for AAV-CIRTS-gRNA9 and AAV-
136 CIRTS-gRNA21, using AAV9 as a gold-standard comparison. At P0, *Scn1a*$^{+/-}$ mice received an
137 intracerebroventricular (ICV) and intravenous (IV) delivery of either AAV-F (7x10^{10} vg/pup) or
138 AAV9 (7x10^{11} vg/pup), each encoding either gRNA9 or 21 to determine the effects on survival.
139 This study was fully blinded and randomised (Fig. 2A). AAV-F vectors were injected at 10-fold
140 lower dose than AAV9, we have previously demonstrated a greater CNS transduction of AAV-F
141 at a 10-fold lower dose after neonatal ICV delivery*(20)*. Furthermore, here in this study, we
142 demonstrated a superior biodistribution in the brain and visceral organs with AAV-F compared
143 to titre matched AAV9 (Fig S4) after neonatal IV delivery. In addition, AAV-F displayed a
144 greater transduction of neurons and astrocytes compared to AAV9 (Fig. S5 & S6).

145 PBS-injected *Scn1a*$^{+/+}$ and *Scn1a*$^{+/-}$ mice served as controls. *Scn1a*$^{+/-}$ mice treated with AAV-F-
146 CIRTS-gRNA9 had a significant (P=0.0235) increase in overall survival to 70.4% at P100
147 compared to 36.4% survival at P100 in PBS-treated *Scn1a*$^{+/-}$ controls (Fig. 2A). In contrast,
148 AAV9-CIRTS-gRNA9 only showed an overall survival of 26.5% (P=0.8439, Fig. 2A). The
149 AAV-F-CIRTS-gRNA21 treatment group also appeared less efficient, showing only a 12.5%
150 survival (P=0.0509, Fig. S8A), while AAV9-CIRTS-gRNA21 had a 50% survival at P100

151 (P=0.3715, Fig. S8A). Weights and open field analysis of neither AAV-F- or AAV9-CIRTS-
152 gRNA9/21 treated mice differed from PBS *Scn1a*$^{+/+}$ and *Scn1a*$^{+/-}$ control group (Fig. 2D, Fig.
153 S7A & Fig. S8C and D). From these data, AAV9 RNA editing at a 10-fold higher titre than
154 AAV-F failed to improve survival we therefore, proceeded with AAV-F-CIRTS-gRNA9 for the
155 remaining experiment.

156 We interrogated dose-range efficacy of AAV-F-CIRTS-gRNA9 with one higher and one
157 lower dose. High dose (1.75x10^{11} vg/pup) resulted in 65.5% survival (P=0.0732, Fig. 3A), whilst
158 low dose (1.75x10^{10} vg/pup) resulted in 44.4% survival, compared to PBS-treated *Scn1a*$^{+/-}$ mice
159 over 100 days (P=0.5815 and P=0.8556, respectively, Fig. 3A). Neither of the additional AAV-
160 F-CIRTS-gRNA9 doses were superior to our originally tested dose of 7x10^{10} vg/pup.
161 Furthermore, no doses showed difference in weight or open field assessment compared to PBS
162 *Scn1a*$^{+/+}$ control group (Fig. 3B, C and Fig. S9A).

163

164 **AAV-F-CIRTS-gRNA9 reduces seizure burden in DS mice**

165 To assess the effects of this optimal dose of AAV-F-CIRTS-gRNA9 therapy on febrile
166 and spontaneous seizures in *Scn1a*$^{+/-}$ mice, we administered a separate cohort of *Scn1a*$^{+/-}$ mice
167 with neonatal ICV and IV delivery (7x10^{10} vg/pup). We also administered control groups AAV-
168 F-CIRTS-gRNAluc (7x10^{10} vg/pup) and PBS to neonatal *Scn1a*$^{+/-}$ mice via ICV and IV delivery
169 (Fig. 4A). Febrile seizure assessment revealed a significant improvement in seizure severity
170 determined by the Racine scale*(31)* (Fig. 4B), in AAV-F-CIRTS-gRNA9 treated *Scn1a*$^{+/-}$ mice
171 compared to PBS *Scn1a*$^{+/-}$ control group (P<0.0001; Fig. 4B), and AAV-F-CIRTS-gRNAluc
172 *Scn1a*$^{+/-}$ control group (P=0.0111; Fig. 4B).

173 Electroencephalogram (EEG) recordings of spontaneous seizures were recorded for 15
174 days between P30-45 and the results revealed a trend to reduction of seizure burden in AAV-F-
175 CIRTS-gRNA9 mice, compared to a control AAV-F-CIRTS-gRNAluc. Total numbers of
176 seizures (9.7±13 vs 4.1±7.3; P=0.4121; Fig. S10A) and average numbers of seizures per day
177 (0.78±0.93 vs 0.33±0.48; P=0.43; Fig. S10B) were reduced. In the mice which displayed
178 seizures, the average seizure duration was significantly reduced in the treated AAV-F-CIRTS-
179 gRNA9 *Scn1a*$^{+/-}$ group compared to control AAV-F-CIRTS-gRNAluc *Scn1a*$^{+/-}$ group (P=0.0279;
180 Fig. 4D), as well as a trend for reduction in cumulative seizure time (P=0.0640; Fig. S10C).

181

182 **AAV-F-CIRTS-gRNA9 normalises molecular signature of DS**

183 To determine the effects of AAV-F-CIRTS-gRNA9 on endogenous *Scn1a* mRNA, we
184 assessed gene expression in the cortex and the heart of treated *Scn1a*$^{+/-}$ mice. Raw wild-type
185 *Scn1a* gene expression levels were restored in both the cortex and heart of AAV-F-CIRTS-
186 gRNA9 mice (P=0.0072 and P=0.0002 vs PBS *Scn1a*$^{+/-}$; Fig. 5A and B).

187 Vector copy number (VCN) assessing the presence of the effector protein *YTHDF2*
188 genomic sequence, showed an increase in both *Scn1a*$^{+/-}$ and *Scn1a*$^{+/+}$ mice treated with AAV-F-
189 CIRTS-gRNA9 treated mice in the cortex at P100 compared to both PBS (P=0.0014) and AAV-
190 F-CIRTS-gRNAluc (P=0.0146) groups *Scn1a*$^{+/+}$ (VCN 0.35±0.44; Fig. 5C). No difference was
191 observed in the heart and the liver (VCN 0.19±0.14 and 0.04±0.05, respectively; Fig. 5C).
192 *YTHDF2* mRNA expression mimicked the pattern of vector copy number with highest
193 expression in the cortex in AAV-F-CIRTS-gRNA9 *Scn1a*$^{+/-}$ mice. No significance was observed
194 in the heart and the liver (Fig. S11A).

195 ***In vivo* safety of AAV-F-CIRTS-gRNA9**

196 Both AAV-F-CIRTS-gRNA9 and AAV-F-CIRTS-gRNAluc were injected to *Scn1a*$^{+/+}$
197 mice at the two highest dosages 1.75x10^{11} vg/pup and 7x10^{10} vg/pup via neonatal ICV and IV to
198 determine any toxicological findings. No adverse effects on survival or weight were seen (Fig.
199 S12A and B). Open field analyses revealed hyperactivity in the total distance of *Scn1a*$^{+/+}$ AAV-
200 F-CIRTS-gRNAluc mice treated with dose 1.75x10^{11} vg/pup at P18 and P55 (P=0.0003,
201 P=0.0217; Fig. S12C), also with an increase in maximum speed at P55 (P=0.0099; Fig. S12D)
202 compared to PBS *Scn1a*$^{+/+}$ control group.

203 Immunohistochemical analysis to detect astrocytes (GFAP) and macrophages, including
204 kupffer cells, in the brain and liver respectively was performed post-AAV-F-CIRTS-gRNA9
205 treatment. No increases in reactive astrocytes were seen in the brains of treated *Scn1a*$^{+/+}$ or
206 *Scn1a*$^{+/-}$ mice (Fig. 6A and B). An increase in the presence of macrophages/kupffer cells in the
207 liver was seen in only the *Scn1a*$^{+/+}$ mice treated with AAV-F-CIRTS-gRNAluc (P=0.0025), this
208 was not observed in mice of either genotype treated with the same dose of AAV-F-CIRTS-
209 gRNA9 (Fig. 6A and C).

210

211 ***In vivo* editing specificity of AAV-F-CIRTS-gRNA9**

212 To identify gRNA-specific changes in gene expression, we conducted RNA-seq on
213 cortical tissue 50 days post-injection and compared AAV-F-CIRTS-gRNAluc and AAV-F-
214 CIRTS-gRNA9 *Scn1a*$^{+/-}$ mice. Only 9 differentially expressed genes were found; 3 up-regulated
215 and 6 down-regulated (Fig. 7A and B). Of note, inflammation-associated genes were down-
216 regulated including *Igkc* (-7.27Log2FC, P=0.0417), *Cxcl13* (-7.35Log2FC, P=0.0417) and *Adgre*

217 (-1.86Log2FC, P=0.0019) and the only driver GO term changed across the comparison, was the
218 down-regulation of CXCR5 chemokine receptor binding (Fig. 7C; P=0.0499). None of the *Scna*
219 genes, which encode other voltage-gated sodium ion channels, were differentially expressed in
220 the gRNA9 group compared to gRNAluc.

221

222

223 **DISCUSSION**

224 Here, we provide preclinical proof-of-concept data demonstrating that CIRTS-mediated
225 RNA editing can mitigate the phenotype of a severe neurological disorder, Dravet syndrome. A
226 single administration of AAV-F-CIRTS-gRNA9 by combined ICV and IV delivery to *Scn1a*$^{+/-}$
227 DS mice induces destruction of *Scn1anat* and completely rescues endogenous *Scn1a* mRNA
228 expression in both the cortex and the heart. This was shown to improve disease manifestation by
229 reducing febrile seizure severity and significantly reducing SUDEP, with minimal off-target
230 effects; whilst being compromised entirely of human components.

231 We designed the gRNAs used in this study with the aim of restoring wild-type *Scn1a*
232 expression levels, without leading to supraphysiological expression. Notably, modest 2.6- and
233 1.9-fold increase of *Scn1a* expression *in vitro* were achieved with gRNA21 and gRNA9
234 respectively. We sought to combine these with AAV-F, an engineered capsid, shown to have a
235 more efficient CNS transduction profile than AAV9 in rodents*(32)*, human neurons*(32)* and
236 NHPs*(19)*. Furthermore, we have validated this with neonatal delivery both by ICV*(20)* and IV
237 delivery. By packaging AAV-CIRTS-gRNA9 into AAV-F and AAV9 we demonstrated vastly
238 different therapeutic effects with 70.4% and 26.5% survival, respectively, strikingly this was
239 achieved with AAV-F being administered at a 10-fold lower dose. However, gRNA21 delivered
240 by either AAV-F or AAV9 did not reveal a significant improvement in survival. We tested a

241 varying dose of AAV-F-CIRTS-gRNA9 and determined that $7x10^{10}$ vg/pup achieved a
242 significant survival of 70.4% at P100, interestingly increasing the dose further to $1.75x10^{11}$
243 vg/pups showed a reduced survival of 65.5% over 100 days. These findings suggest a narrow
244 therapeutic dose ranging window for a successful treatment for DS. This is particularly important
245 in the context of *SCN1A*, as gain-of-function *SCN1A* variants, which are known to cause familial
246 hemiplegic migraine type 3 and a severe infantile developmental and encephalopathy (distinct
247 from DS) with associated movement disorder*(33)*. Therefore, future studies require a more
248 refined dose ranging evaluation of AAV-F with gRNA9 or gRNA21 to determine the optimal
249 therapeutic dose, with appropriate levels of physiological *Scn1a* and no behavioural side effects.

250 As a main symptom of DS is seizures, we sought to assess the seizure activity in our
251 AAV-F-CIRTS-gRNA9 treated *Scn1a*$^{+/-}$ DS mice via febrile seizure assessment and EEG
252 monitoring for 15 days (P30-45). We delivered a vehicle and control vector AAV-F-CIRTS-
253 gRNAluc to *Scn1a*$^{+/-}$ DS mice as a comparators. Febrile seizure assessment revealed a
254 significant reduction in seizure severity determined by the Racine scale in AAV-F-CIRTS-
255 gRNA9 treated *Scn1a*$^{+/-}$ mice compared to PBS and AAV-F-CIRTS-gRNAluc *Scn1a*$^{+/-}$ control
256 group. EEG seizure monitoring was performed for AAV-F-CIRTS-gRNA9 and AAV-F-CIRTS-
257 gRNAluc treated *Scn1a*$^{+/-}$ DS mice. Our results showed that we could significantly reduce the
258 seizure duration in our treated *Scn1a*$^{+/-}$ DS mice. From these data, we observed a variability in
259 the AAV-F-CIRTS-gRNAluc *Scn1a*$^{+/-}$ DS mice, as some of these mice did not display seizures
260 during the EEG recording. Which may partly be due to the variable penetrance of spontaneous
261 seizures in this model*(34)*. This was a limitation in our study and future studies, will require
262 further power calculations to establish the appropriate number of *Scn1a*$^{+/-}$ mice required for EEG
263 seizure monitoring.

264 Molecular assessment revealed a significant increase in endogenous *Scn1a* mRNA in the
265 cortex and the heart of treated AAV-F-CIRTS-gRNA9 *Scn1a*$^{+/-}$ mice. Immunohistochemical
266 analysis in the brain of AAV-F-CIRTS-gRNA9 *Scn1a*$^{+/-}$ and *Scn1a*$^{+/+}$ mice showed no signs of
267 toxicity. Liver toxicity was only observed in AAV-F-CIRTS-gRNAluc *Scn1a*$^{+/+}$ treated group,
268 suggesting potential guide-specific side-effects of AAV-F-CIRTS-gRNAluc vector.

269 To determine the off-target effects of our gRNA9, we conducted RNA-seq on cortical
270 brain tissues for AAV-F-CIRTS-gRNAluc and AAV-F-CIRTS-gRNA9 *Scn1a*$^{+/-}$ treated mice.
271 The data revealed inflammation-associated genes including *Igkc(35)*, *Cxcl13(36)* and *Adgre(37)*
272 were down-regulated in the AAV-F-CIRTS-gRNA9 treated group. Previously, up-regulation of
273 the CXCL13-CXCR5 signalling pathway has been associated with intractable epilepsy*(36)*,
274 suggesting that our therapy may be able to reduce some molecular signatures of epilepsy
275 pathogenesis. Furthermore, our data suggest no off-target effects of the gRNA9 coupled with the
276 CIRTS machinery.

277 Several approaches in preclinical development have used genetic therapies specifically in
278 inhibitory interneurons using *SCN1A* gene replacement with split-intein dual AAVs*(38)* and
279 Adenoviral vectors*(39)*, CRISPR/dCas9 activation of *SCN1A(40, 41)* and transcription factor-
280 mediated *SCN1A* up-regulation*(30)*. While these approaches target the primary pathology of
281 Dravet syndrome (DS), our strategy complements these alternative therapeutic interventions by
282 also considering effects in less well-studied cell populations, such as cardiomyocytes*(10)*. Here,
283 we have shown that our AAV-F-CIRTS-gRNA9 can increase *Scn1a* mRNA in the cortex and the
284 heart.

285 *SCN1ANAT* has been detected in surgical brain tissue specimens from patients (1-19
286 years of age) undergoing resection to treat refractory, non-DS epilepsy*(42)*. Previous evidence

287 has shown that targeting *Scn1anat* using small oligonucleotides termed AntagoNATs were able
288 to reduce seizures and normalise neuronal activity in DS knock-in mice*(27)*. Furthermore, we
289 have also shown that these AntagoNATs can be vectorised with AAV9, which also demonstrates
290 a significant improvement in DS phenotype*(43)*. Here, we also are targeting *Scn1anat*, but
291 instead of blocking the interaction between this and the *Scn1a* mRNA, we are inducing the
292 degradation of *Scn1anat*, with similar phenotypic improvement. These findings demonstrate the
293 feasibility of using AAV mediated RNA editing to modulate *Scn1a* expression, highlighting its
294 potential as a therapeutic for DS.

295 Genetic therapies for DS have progressed to clinical evaluation. These include the
296 antisense oligonucleotide (ASO) zorevunersen, currently under investigation in Phase 1/2a
297 MONARCH and ADMIRAL trials, which involve repeated intrathecal administration*(44)*.
298 Encoded Therapeutics has developed an AAV9-based transcription factor*(30)* approach
299 specifically targeting GABAergic interneurons, now being assessed in a Phase 1/2 clinical trial
300 utilizing ICV delivery alone*(45)*. Similar to Encoded Therapeutics' strategy, our AAV-F-CIRTS-
301 gRNA9 platform offers a one-time treatment; however, it confers the additional advantage of
302 enabling broader targeting of CNS cell populations expressing Nav1.1. Furthermore, the
303 inclusion of IV administration is intended to achieve efficient cardiac transduction, addressing
304 evidence implicating altered cardiac electrophysiology*(8, 11)* in contributing to SUDEP.

305 Our study presented limitations. Some of the *Scn1a*$^{+/-}$ DS mice did not present seizures
306 during EEG recording and therefore, for future studies we will require further power
307 calculations. The future studies required have been detailed in this discussion.

308 In conclusion, we have developed and characterized an AAV-F-CIRTS RNA editing
309 therapeutic strategy for the treatment of DS. Incorporation of gRNA targeting *Scn1anat*

310 successfully modulated *Scn1a* expression and significantly improved survival, seizure severity
311 and duration in *Scn1a*$^{+/-}$ mice. These findings provide compelling proof-of-concept evidence
312 supporting the potential of this approach as a therapeutic intervention for DS.

313

314

315 **MATERIALS AND METHODS**

316 **Study design**

317 This study was designed to investigate if AAV-CIRTS-mediated RNA editing to induce
318 the destruction of *Scn1anat* could lead to therapeutic benefit in a clinically relevant DS mouse
319 model. The following design elements were included in this study. N=3 independent experiments
320 were conducted for *in vitro* gRNA screening experiments with at least n=3 technical replicates
321 per condition. Mice were assigned randomly to study groups, with at least one control (either
322 PBS or AAV-F-CIRTS-gRNAluc-treated) *Scn1a*$^{+/-}$ mouse per litter and remaining *Scn1a*$^{+/+}$ and
323 *Scn1a*$^{+/-}$ littermates mice treated with AAV-F-CIRTS-gRNA9/21 or AAV9-CIRTS-gRNA9/21
324 treated mouse. Prospectively selected endpoints of these studies were survival, weight, open
325 field, longitudinal gene expression and neuropathological analyses. Sample sizes for *in vivo*
326 experiments were not pre-defined before the outset of data collection as no preliminary data were
327 available to estimate effect sizes and thus be able to complete power analyses. *In vivo* studies
328 analysing seizures used *Scn1a*$^{+/-}$ littermates treated with AAV-F-CIRTS-gRNAluc as a non-
329 targeting guide as a control for AAV-F-CIRTS-gRNA9. At termination of the in-life period for
330 all *in vivo* experiments, mice were assigned a numeric code and investigators were blinded to
331 treatment and genotype whilst analysing tissue.

332 **gRNA design and cloning**

333 The *Scn1anat* target sequence was inputted into sOligo software
334 (https://sfold.wadsworth.org/cgi-bin/soligo.pl), varying the parameter for gRNA length. Folding
335 temperature was set to 37°C and ionic conditions set to 1M NaCl with no divalent ions.
336 Resulting outputs were screened for those with less than -8.0 Gibbs free energy with positional
337 clusters identified. Potential gRNA sequences were manually mapped to RNA secondary
338 structures produced using mFold software (http://www.unafold.org/mfold/applications/rna-
339 folding-form.php) to determine qualities of each gRNA such as the number of termini and
340 percentage of gRNA sequence in open conformation. gRNAs were cloned into the AAV-CIRTS
341 plasmid (Addgene plasmid #132544), using gBlocks from Integrated DNA Technologies and
342 InFusion cloning (Takara Bio). The AAV-CIRTS plasmid contains a cytomegalovirus promoter
343 (CMV), driving ssRNA binding protein β-defensin 3, RNA hairpin-binding protein (TBP6.7),
344 effector protein (YTHDF2) and U6 promoter driving gRNA (referred to as AAV-CIRTS in the
345 main text, Fig. 1B).

346 ***In vitro* analyses**

347 For luciferase assays; HEK293T cells ($5x10^4$ per well of 24-well plate) were transfected
348 with 0.8μg of an AAV plasmid containing an Spleen focus forming virus ubiquitous promoter
349 (SFFV) driving luciferase linked to green fluorescent reporter gene with a T2A linker
350 peptide*(46)* (referred to as AAV-SFFV-*luciferase*-T2A-*eGFP* in the main text) ± 0.8μg AAV-
351 CIRTS-gRNAluc using Lipofectamine 2000 (Thermo Fisher Scientific). Cells were lysed in
352 Luciferase Cell Culture Lysis Reagent (Promega) at 72h post-transfection, with half the lysate
353 used to determine protein concentration using the DC protein assay (BioRad). The remaining
354 half of the lysate was used for luminometry measured in a FLUOstar® Omega microplate

355 reader (BMG Labtech). Luciferase expression was normalised to protein concentration within
356 each sample.

357 For *Scn1anat* gRNA screening; Neuro2a cells ($3x10^4$ per well of 24-well plate) were
358 differentiated in DMEM (Thermo Fisher Scientific), 2% FCS (Sigma-Aldrich), 0.5mM cAMP
359 (Merck) and 20µM Retinoic Acid (Merck). At 6DIV, cells were transfected with 0.8µg AAV-
360 SFFV-*luciferase*-T2A-*eGFP* or AAV-CIRTS-gRNA1-21 using Lipofectamine 2000 (Thermo
361 Fisher Scientific). Cells were lysed in TRIzol reagent (Thermo Fisher Scientific) at 5d post-
362 transfection. RNA was extracted and qPCR used to determine changes in *Scn1a* gene expression
363 (protocols described below).

364 **AAV vector production**

365 Recombinant AAV vectors were produced by triple-transfection*(47)* of AAVpro 293T
366 cells (Takara Bio) with AAV-CIRTS, adenovirus helper plasmid (Harvard University) and either
367 AAV9 (University of Pennsylvania; Addgene #112865) or AAV-F (Harvard University,
368 Addgene #166921) capsid plasmids using PEImax (Polysciences Inc.). HPLC using POROS
369 CaptureSelect AAVX Resin (Thermo Fisher Scientific) was used to purify resulting vector
370 before being titrated by qPCR.

371 **Animals**

372 All procedures were performed in accordance with UK Home Office Animals (Scientific
373 Procedures) Act 1986 under PPLs 70/14300, PP8023218 & PP9223137. All mice were housed in
374 IVCs with enrichment, under a 12 hour:12 hour light–dark cycle and had access to food and
375 water *ad libitum*. The mouse model of Dravet syndrome used in this project is derived from the
376 129Sv-*Scn1a*^{tm1Kea}/Mmjax model*(28, 29)* (Jackson Laboratory) that has been extensively used in

377 DS pre-clinical research. Males from this strain were bred with wild-type CD1 females to obtain
378 a F1 129Sv-*Scn1a*^{tm1Kea}/Mmjax x CD1 generation. F1xF1 crosses were bred to obtain F2 129Sv-
379 *Scn1a*^{tm1Kea}/Mmjax x CD1 heterozygote females which were bred to wild-type C57BL/6J males
380 to obtain experimental litters (here referred to as *Scn1a*$^{+/-}$ in the text). Humane endpoints of
381 >15% weight loss, observation of two seizures and/or clear signs of illness (piloerection,
382 hunched posture and laboured breathing).

383 At post-natal day 0 (P0), *Scn1a*$^{+/-}$ pups were injected by bilateral intracerebroventricular
384 (ICV; 5 µL per hemisphere, using previously published coordinates*(48)*) and intravenous (IV; 25
385 µL via superficial temporal vein*(49)*) routes of administration with either PBS, AAV9 (total dose
386 $7x10^{11}$ vg/pup ($2x10^{11}$ vg ICV + $5x10^{11}$ vg IV)) or AAV-F (total dose $1.75x10^{10}$ vg/pup ($5x10^{9}$
387 vg ICV + $1.25x10^{10}$ vg IV), $7x10^{10}$ vg/pup ($2x10^{10}$ vg ICV + $5x10^{10}$ vg IV) and $1.75x10^{11}$
388 vg/pup ($5x10^{10}$ vg ICV + $1.25x10^{11}$ vg IV)) using a 33-gauge Hamilton needle (VWR). For the
389 biodistribution study AAV9 ($1.9x10^{10}$ and $1.9x10^{11}$ vg/pup) and AAV-F ($1.9x10^{10}$ vg/pup) was
390 delivered intravenously via superficial temporal vein*(49)*). After the procedure, mice were
391 returned to their dams. Weight and survival were monitored until endpoint.

392 Open field analysis with 15 minutes free locomotion was completed at P18, P38, P55 and
393 P75 using SMART v3 software (Harvard Panlab). At endpoint, tissues were collected by snap-
394 freezing or fixing in 4% PFA.

395 **EEG recordings**

396 AAV-F-CIRTS-gRNAluc and AAV-F-CIRTS-gRNA9 treated *Scn1a*$^{+/-}$ mice underwent
397 EEG recordings from P30-P45 using wireless electrocorticogram (ECoG) transmitters (Cat. No.

398 A3048P2-AA-C37-D, single-channel transmitter, Open Source Instruments), as previously
399 described*(43)*.

400 **RNA/DNA extraction, gene expression and VCN**

401 RNA extraction was completed using the PureLink kit (Thermo Fisher Scientfic), DNA
402 extraction was completed using DNeasy Blood & Tissue kit (Qiagen), as previously
403 described*(43)*. The following primers and probes were used to quantify gene expression, titrate
404 AAV vectors and perform vector copy number analyses. *Scn1a;* forward:
405 TCAGAGGGAAGCACAGTAGAC, reverse: TTCCACGCTGATTTGACAGCA, probe:
406 CCAGAAGAAACCCTTGAGCCCGAA (fluorophore: ABY, quencher: QSY, Thermo Fisher
407 Scientific). *Gapdh*; forward: ACGGCAAATTCAACGGCAC, reverse:
408 TAGTGGGGTCTCGCTCCTGG, probe: TTGTCATCAACGGGAAGCCCATCA (fluorophore:
409 VIC, quencher: QSY, Thermo Fisher Scientific). *YTHDF2*; forward:
410 CCTCCATTGGCTTCTCCTATTC, reverse: GTTGCTCAGCTGTCCATAAGA, probe:
411 TTAAGTAGGGCATGGCTGTGTCACC (fluorophore: FAM, quencher: ZEN / Iowa Black™
412 FQ, Integrated DNA Technologies).

413 The same sequence *Gapdh* primers and probe, and *Scn1a* primers were used for ddPCR
414 analysis, but with the *Scn1a* probe fluorophore was adapted from ABY to FAM. 5µL of each
415 cDNA (equivalent to 85 pg) was loaded per reaction with 1X ddPCR Multiplex Supermix (Bio-
416 Rad) and 4 mM DTT. ddPCR analysis was performed using the BioRad QXOne in the UCL
417 NeuroGTx Vector Core Facility. The Facility is supported by the NIHR Great Ormond Street
418 Hospital Biomedical Research Centre. The views expressed are those of the author(s) and not
419 necessarily those of the NHS, the NIHR or the Department of Health.

420 **Immunoperoxide staining**

421 40 µm coronal sections cut using a Micron HM 430 freezing microtome (Thermo Fisher
422 Scientific) were analysed using previously published protocols*(43)*. Neuropathological analyses
423 used the following primary antibodies; anti-GFAP (Proteintech 16825-1-AP; 1:2000) and anti-
424 CD68 (BioRad MCA1957; 1:100). Images were acquired using a Leica Microsystems
425 stereoscopic microscope (DM4000), Leica DFC7000T camera and Leica LAX X software (all
426 Leica Microsystems UK). Images were background corrected using FIJI (ImageJ) and
427 thresholding software (Image-Pro Premier v10; Media Cybernetics) was used to quantify
428 expression.

429 **Immunofluorescence staining**

430

431 40 µm coronal sections were used*(43)*. Immunolabeling was performed on free-floating
432 sections using antibodies against GFP (Abcam; ab290), NeuN (Merek; MAB377) and GFAP
433 (Proteintech; 16825-1-AP)*(20)*. Images were assessed using fluorescence microscope (Leica
434 DFC7000 7) using LAS X Microscope Software (Leica Microsystems). The percentage of GFP
435 positive neurons and astrocytes were analysed using the CellProfiler Software (Broad Institute
436 2021). The images were overlayed using ImageJ.

437 **RNA-seq**

438 Total RNA was extracted from the cortex of *Scn1a*$^{+/+}$ and *Scn1a*$^{+/-}$ P50 mice that were
439 controls, or had been treated with, AAV-F-CIRTS-gRNAluc or AAV-F-CIRTS-gRNA9.

440 Untreated control samples were processed by UCL Genomics using a KAPA mRNA
441 HyperPrep and NextSeq2000 P2 100c configuration with single-end reads at 25M reads/sample.
442 N=8 mice per genotype were submitted, but due to a pooling error, *Scn1a*$^{+/+}$ Untreated_5 could
443 not be included in the analysis.

444 AAV-CIRTS-treated samples (n=4 per group) were processed by Azenta Life Sciences
445 using Illumina NovaSeq with paired-end reads in 2x150 bp configuration. Trimmomatic v.0.36
446 was used to trim sequence reads to remove adapter sequences before reads were mapped to *Mus*
447 *musculus* GRCm38 reference genome using the STAR aligner v.2.5.2b. Unique gene counts
448 were extracted using featureCounts (Subread package v.1.5.2).

449 Both RNA-seq analyses then used DESeq2*(50)* to determine differential gene expression
450 analysis. Untreated samples were subjected to an absolute Log2 fold change > 0.7, whilst AAV-
451 CIRTS comparisons used an absolute Log2 fold change > 1. In both analyses, genes with an
452 adjusted P value < 0.05 were called differentially expressed genes. A gene ontology analysis was
453 performed on the statistically significant set of genes by implementing enrichGO and
454 clusterProfiler R packages*(51)* to cluster the set of genes based on their molecular function and
455 determine their statistical significance.

456 **Statistical analyses**

457 GraphPad Prism (version 10.3.1, Boston) was used for statistical analyses. All continuous
458 variables are presented as mean±SD in graphs. *In vitro* data were analysed using an unpaired,
459 two-tailed t-test for luciferase assay or one-way ANOVA with Dunnett's multiple comparisons
460 for gRNA screening. Survival was determined using a Log-rank (Mantel-Cox) test. Weights
461 were initially screened for differences with one-way ANOVA with Dunnett's multiple
462 comparisons for group-group comparisons and a mixed-effect analysis was completed with
463 analysis at each individual timepoint. Groups were excluded in mixed-effect analyses from the
464 timepoint that only a single mouse remained. Open field was analysed using two-way ANOVA
465 with Dunnett's multiple comparisons. Racine scaling of febrile seizures were contingency
466 analysed with Fisher's exact test. A mixed-effects analysis was used to compare overall EEG

467 seizure burden, with either Mann-Whitney or unpaired, two-tailed t-test for individual seizure

468 readouts. One-way and two-way ANOVAs were used to analyse all molecular data.

469 **Supplementary Materials**

470 PDF file includes;

471 Fig S1 to S12 supplementary figures

472

473 **REFERENCES**

474 1. E. Chilcott, J. A. Díaz, C. Bertram, M. Berti, R. Karda, Genetic therapeutic advancements for Dravet Syndrome.
475 *Epilepsy & Behavior* **132**, 108741 (2022).

476 2. A. Strzelczyk, L. Lagae, J. Wilmshurst, A. Brunklaus, P. Striano, F. Rosenow, S. Schubert-Bast, Dravet
477 syndrome: a systematic literature review of the illness burden. *Epilepsia Open* (2023).

478 3. A. Brunklaus, S. M. Zuberi, Dravet syndrome—From epileptic encephalopathy to channelopathy. *Epilepsia* **55**,
479 979–984 (2014).

480 4. M. Wolff, C. Cassé-Perrot, C. Dravet, Severe myoclonic epilepsy of infants (Dravet syndrome): natural history
481 and neuropsychological findings. *Epilepsia* **47 Suppl 2**, 45–48 (2006).

482 5. A. Brunklaus, E. Pérez-Palma, I. Ghanty, J. Xinge, E. Brilstra, B. Ceulemans, N. Chemaly, I. de Lange, C.
483 Depienne, R. Guerrini, D. Mei, R. S. Møller, R. Nabbout, B. M. Regan, A. L. Schneider, I. E. Scheffer, A.-S.
484 Schoonjans, J. D. Symonds, S. Weckhuysen, M. W. Kattan, S. M. Zuberi, D. Lal, Development and Validation of a
485 Prediction Model for Early Diagnosis of SCN1A-Related Epilepsies. *Neurology* **98**, e1163–e1174 (2022).

486 6. S. Gataullina, O. Dulac, From genotype to phenotype in Dravet disease. *Seizure* **44**, 58–64 (2017).

487 7. W. R. J. Whitaker, R. L. M. Faull, H. J. Waldvogel, C. J. Plumpton, P. C. Emson, J. J. Clare, Comparative
488 distribution of voltage-gated sodium channel proteins in human brain. *Molecular Brain Research* **88**, 37–53 (2001).

489 8. A. T. Berg, K. Coffman, D. Gaebler-Spira, Dysautonomia and functional impairment in rare developmental and
490 epileptic encephalopathies: the other nervous system. *Developmental Medicine & Child Neurology* **63**, 1433–1440
491 (2021).

492 9. F. Kalume, R. E. Westenbroek, C. S. Cheah, F. H. Yu, J. C. Oakley, T. Scheuer, W. A. Catterall, Sudden
493 unexpected death in a mouse model of Dravet syndrome. *J Clin Invest* **123**, 1798–1808 (2013).

494 10. S. Mishra, V. Reznikov, V. A. Maltsev, N. A. Undrovinas, H. N. Sabbah, A. Undrovinas, Contribution of
495 sodium channel neuronal isoform Nav1.1 to late sodium current in ventricular myocytes from failing hearts. *The*
496 *Journal of Physiology* **593**, 1409–1427 (2015).

497 11. D. S. Auerbach, J. Jones, B. C. Clawson, J. Offord, G. M. Lenk, I. Ogiwara, K. Yamakawa, M. H. Meisler, J. M.
498 Parent, L. L. Isom, Altered Cardiac Electrophysiology and SUDEP in a Model of Dravet Syndrome. *PLOS ONE* **8**,
499 e77843 (2013).

500 12. A. Strzelczyk, S. Schubert-Bast, A Practical Guide to the Treatment of Dravet Syndrome with Anti-Seizure
501 Medication. *CNS Drugs* **36**, 217–237 (2022).

502 13. G. Massaro, C. N. Z. Mattar, A. M. S. Wong, E. Sirka, S. M. K. Buckley, B. R. Herbert, S. Karlsson, D. P.
503 Perocheau, D. Burke, S. Heales, A. Richard-Londt, S. Brandner, M. Huebecker, D. A. Priestman, F. M. Platt, K.
504 Mills, A. Biswas, J. D. Cooper, J. K. Y. Chan, S. H. Cheng, S. N. Waddington, A. A. Rahim, Fetal gene therapy for
505 neurodegenerative disease of infants. *Nature Medicine* (2018), doi:10.1038/s41591-018-0106-7.

506 14. J. Ng, S. Barral, C. de la Fuente Barrigon, G. Lignani, F. A. Erdem, R. Wallings, R. Privolizzi, G. Rossignoli, H.
507 Alrashidi, S. Heasman, E. Meyer, A. Ngoh, S. Pope, R. Karda, D. Perocheau, J. Baruteau, N. Suff, J. A. Diaz, S.
508 Schorge, J. Vowles, L. R. Marshall, S. A. Cowley, S. Sucic, M. Freissmuth, J. R. Counsell, R. Wade-Martins, S. J.
509 R. Heales, A. A. Rahim, M. Bencze, S. N. Waddington, M. A. Kurian, Gene therapy restores dopamine transporter
510 expression and ameliorates pathology in iPSC and mouse models of infantile parkinsonism. *Science Translational*
511 *Medicine* **13**, 1–13 (2021).

512 15. J. R. Mendell, S. Al-Zaidy, R. Shell, W. D. Arnold, L. R. Rodino-Klapac, T. W. Prior, L. Lowes, L. Alfano, K.
513 Berry, K. Church, J. T. Kissel, S. Nagendran, J. L'Italien, D. M. Sproule, C. Wells, J. A. Cardenas, M. D. Heitzer,
514 A. Kaspar, S. Corcoran, L. Braun, S. Likhite, C. Miranda, K. Meyer, K. D. Foust, A. H. M. Burghes, B. K. Kaspar,
515 Single-Dose Gene-Replacement Therapy for Spinal Muscular Atrophy. *New England Journal of Medicine* **377**,
516 1713–1722 (2017).

517 16. K. A. Strauss, M. A. Farrar, F. Muntoni, K. Saito, J. R. Mendell, L. Servais, H. J. McMillan, R. S. Finkel, K. J.
518 Swoboda, J. M. Kwon, C. M. Zaidman, C. A. Chiriboga, S. T. Iannaccone, J. M. Krueger, J. A. Parsons, P. B. Shieh,
519 S. Kavanagh, S. Tauscher-Wisniewski, B. E. McGill, T. A. Macek, Onasemnogene abeparvovec for presymptomatic
520 infants with two copies of SMN2 at risk for spinal muscular atrophy type 1: the Phase III SPR1NT trial. *Nat Med* **28**,
521 1381–1389 (2022).

522 17. D. Chand, F. Mohr, H. McMillan, F. F. Tukov, K. Montgomery, A. Kleyn, R. Sun, S. Tauscher-Wisniewski, P.
523 Kaufmann, G. Kullak-Ublick, Hepatotoxicity following administration of onasemnogene abeparvovec (AVXS-101)
524 for the treatment of spinal muscular atrophy. *Journal of Hepatology* **74**, 560–566 (2021).

525 18. K. S. Hanlon, J. C. Meltzer, T. Buzhdygan, M. J. Cheng, M. Sena-Esteves, R. E. Bennett, T. P. Sullivan, R.
526 Razmpour, Y. Gong, C. Ng, J. Nammour, D. Maiz, S. Dujardin, S. H. Ramirez, E. Hudry, C. A. Maguire, Selection
527 of an Efficient AAV Vector for Robust CNS Transgene Expression. *Molecular Therapy - Methods and Clinical*
528 *Development* **15**, 320–332 (2019).

529 19. A. Beharry, Y. Gong, J. C. Kim, K. S. Hanlon, J. Nammour, K. Hieber, F. Eichler, M. Cheng, A. Stemmer-
530 Rachamimov, K. M. Stankovic, D. B. Welling, C. Ng, C. A. Maguire, The AAV9 Variant Capsid AAV-F Mediates
531 Widespread Transgene Expression in Nonhuman Primate Spinal Cord After Intrathecal Administration. *Hum Gene*
532 *Ther* **33**, 61–75 (2022).

533 20. A. Keegan, O. Cetin, E. M. Chilcott, J. F. Antinao Diaz, S. Eaton, S. N. Waddington, J. R. Counsell, S. Rahman,
534 R. Karda, Next Generation AAV-F Capsid gene therapy rescues disease pathology in a model of Pyruvate
535 Dehydrogenase Complex Deficiency. *bioRxiv* , 2025.07.30.667478 (2025).

536 21. L. E. Burbano, M. Li, N. Jancovski, P. Jafar-Nejad, K. Richards, A. Sedo, A. Soriano, B. Rollo, L. Jia, E.
537 Gazina, S. Piltz, F. Adikusuma, P. Q. Thomas, F. Rigo, C. A. Reid, S. Maljevic, S. Petrou, Antisense
538 oligonucleotide therapy for KCNT1 encephalopathy, 2020.11.12.379164 (2020).

539 22. Z. Han, C. Chen, A. Christiansen, S. Ji, Q. Lin, C. Anumonwo, C. Liu, S. C. Leiser, I. Aznarez, G. Liau, L. L.
540 Isom, *Antisense oligonucleotides increase Scn1a expression and reduce seizures and SUDEP incidence in a mouse*
541 *model of Dravet syndrome* (2020; http://stm.sciencemag.org/), p. 6100.

542 23. D. W. Morgens, M. Wainberg, E. A. Boyle, O. Ursu, C. L. Araya, C. K. Tsui, M. S. Haney, G. T. Hess, K. Han,
543 E. E. Jeng, A. Li, M. P. Snyder, W. J. Greenleaf, A. Kundaje, M. C. Bassik, Genome-scale measurement of off-
544 target activity using Cas9 toxicity in high-throughput screens. *Nat Commun* **8**, 15178 (2017).

545 24. S. Rauch, E. He, M. Srienc, H. Zhou, Z. Zhang, B. C. Dickinson, Programmable RNA-Guided RNA Effector
546 Proteins Built from Human Parts. *Cell* **178**, 122-134.e12 (2019).

547 25. S. Rauch, K. A. Jones, B. Dickinson, Small Molecule-Inducible RNA-Targeting Systems for Temporal Control
548 of RNA Regulation in Vivo (2020), doi:10.26434/chemrxiv.11673711.v1.

549 26. S. U. Madugalle, W.-S. Liau, Q. Zhao, X. Li, H. Gong, P. R. Marshall, A. Periyakaruppiah, E. L. Zajaczkowski,
550 L. J. Leighton, H. Ren, M. R. B. Musgrove, J. W. A. Davies, G. Kim, S. Rauch, C. He, B. C. Dickinson, B.
551 Fulopova, L. N. Fletcher, S. R. Williams, R. C. Spitale, T. W. Bredy, Synapse-Enriched m6A-Modified Malat1
552 Interacts with the Novel m6A Reader, DPYSL2, and Is Required for Fear-Extinction Memory. *J. Neurosci.* **43**,
553 7084–7100 (2023).

554 27. J. Hsiao, T. Y. Yuan, M. S. Tsai, C. Y. Lu, Y. C. Lin, M. L. Lee, S. W. Lin, F. C. Chang, H. Liu Pimentel, C.
555 Olive, C. Coito, G. Shen, M. Young, T. Thorne, M. Lawrence, M. Magistri, M. A. Faghihi, O. Khorkova, C.
556 Wahlestedt, Upregulation of Haploinsufficient Gene Expression in the Brain by Targeting a Long Non-coding RNA
557 Improves Seizure Phenotype in a Model of Dravet Syndrome. *EBioMedicine* **9**, 257–277 (2016).

558 28. A. R. Miller, N. A. Hawkins, C. E. Mccollom, J. A. Kearney, Mapping genetic modifiers of survival in a mouse
559 model of Dravet syndrome. *Genes, Brain and Behavior* **13**, 163–172 (2014).

560 29. A. M. Mistry, C. H. Thompson, A. R. Miller, C. G. Vanoye, A. L. George,, J. A. Kearney, Strain- and age-
561 dependent hippocampal neuron sodium currents correlate with epilepsy severity in Dravet syndrome mice.
562 *Neurobiology of Disease* **65**, 1–11 (2014).

563 30. A. Tanenhaus, T. Stowe, A. Young, J. McLaughlin, R. Aeran, I. W. Lin, J. Li, R. Hosur, M. Chen, J. Leedy, T.
564 Chou, S. Pillay, M. C. Vila, J. A. Kearney, M. Moorhead, A. Belle, S. Tagliatela, Cell-Selective Adeno-Associated
565 Virus-Mediated SCN1A Gene Regulation Therapy Rescues Mortality and Seizure Phenotypes in a Dravet Syndrome
566 Mouse Model and Is Well Tolerated in Nonhuman Primates. *Hum Gene Ther* **33**, 579–597 (2022).

567 31. J. Van Erum, D. Van Dam, P. P. De Deyn, PTZ-induced seizures in mice require a revised Racine scale.
568 *Epilepsy & Behavior* **95**, 51–55 (2019).

569 32. K. S. Hanlon, J. C. Meltzer, T. Buzhdygan, M. J. Cheng, M. Sena-Esteves, R. E. Bennett, T. P. Sullivan, R.
570 Razmpour, Y. Gong, C. Ng, J. Nammour, D. Maiz, S. Dujardin, S. H. Ramirez, E. Hudry, C. A. Maguire, Selection
571 of an Efficient AAV Vector for Robust CNS Transgene Expression. *Mol Ther Methods Clin Dev* **15**, 320–332
572 (2019).

573 33. A. Brunklaus, T. Brünger, T. Feng, C. Fons, A. Lehikoinen, E. Panagiotakaki, M.-A. Vintan, J. Symonds, J.
574 Andrew, A. Arzimanoglou, S. Delima, J. Gallois, D. Hanrahan, G. Lesca, S. MacLeod, D. Marjanovic, A. McTague,
575 N. Nuñez-Enamorado, E. Perez-Palma, M. Scott Perry, K. Pysden, S. J. Russ-Hall, I. E. Scheffer, K. Sully, S. Syrbe,
576 U. Vaher, M. Velayutham, J. Vogt, S. Weiss, E. Wirrell, S. M. Zuberi, D. Lal, R. S. Møller, M. Mantegazza, S.
577 Cestèle, The gain of function SCN1A disorder spectrum: novel epilepsy phenotypes and therapeutic implications.
578 *Brain* **145**, 3816–3831 (2022).

579 34. N. A. Hawkins, L. L. Anderson, T. S. Gertler, L. Laux, A. L. George Jr., J. A. Kearney, Screening of
580 conventional anticonvulsants in a genetic mouse model of epilepsy. *Annals of Clinical and Translational Neurology*
581 **4**, 326–339 (2017).

582 35. J. P. Pandey, P. J. Nietert, A. M. Namboodiri, C. Kimball, P. A. Flume, Roles of immunoglobulin GM and KM
583 allotypes and Fcγ receptor 2 A genotypes in humoral immunity to a conserved microbial polysaccharide in
584 pulmonary diseases. *Genes Immun* **26**, 91–95 (2025).

585 36. R. Li, L. Ma, H. Huang, S. Ou, J. Yuan, T. Xu, X. Yu, X. Liu, J. Yang, Y. Chen, X. Peng, Altered Expression of
586 CXCL13 and CXCR5 in Intractable Temporal Lobe Epilepsy Patients and Pilocarpine-Induced Epileptic Rats.
587 *Neurochem Res* **42**, 526–540 (2017).

588 37. H.-H. Lin, C.-C. Hsiao, C. Pabst, J. Hébert, T. Schöneberg, J. Hamann, in *Advances in Immunology*, G Protein-
589 Coupled Receptors in Immune Response and Regulation. A. K. Shukla, Ed. (Academic Press, 2017), vol. 136, pp.
590 163–201.

591 38. J. K. Mich, J. Ryu, A. D. Wei, B. B. Gore, R. Guo, A. M. Bard, R. A. Martinez, E. M. Luber, J. Liu, Y. M.
592 Bishaw, R. J. Christian, L. M. Oliveira, N. Miranda, J.-M. Ramirez, J. T. Ting, E. S. Lein, B. P. Levi, F. K. Kalume,
593 Interneuron-specific dual-AAV SCN1A gene replacement corrects epileptic phenotypes in mouse models of Dravet
594 syndrome. *Science Translational Medicine* **17**, eadn5603 (2025).

595 39. A. Ricobaraza, M. Bunuales, M. Gonzalez-Aparicio, S. Fadila, M. Rubinstein, I. Vides-Urrestarazu, J. Banderas,
596 N. Sola-Sevilla, R. Sanchez-Carpintero, J. L. Lanciego, E. Roda, A. Honrubia, P. Arnaiz, R. Hernandez-Alcoceba,
597 Preferential expression of SCN1A in GABAergic neurons improves survival and epileptic phenotype in a mouse
598 model of Dravet syndrome. *J Mol Med* **101**, 1587–1601 (2023).

599 40. G. Colasante, G. Lignani, S. Brusco, C. Di Berardino, J. Carpenter, S. Giannelli, N. Valassina, S. Bido, R. Ricci,
600 V. Castoldi, S. Marenna, T. Church, L. Massimino, G. Morabito, F. Benfenati, S. Schorge, L. Leocani, D. M.
601 Kullmann, V. Broccoli, dCas9-Based Scn1a Gene Activation Restores Inhibitory Interneuron Excitability and
602 Attenuates Seizures in Dravet Syndrome Mice. *Molecular Therapy* **28**, 235–253 (2020).

603 41. T. Yamagata, M. Raveau, K. Kobayashi, H. Miyamoto, T. Tatsukawa, I. Ogiwara, S. Itohara, T. K. Hensch, K.
604 Yamakawa, CRISPR/dCas9-based Scn1a gene activation in inhibitory neurons ameliorates epileptic and behavioral
605 phenotypes of Dravet syndrome model mice. *Neurobiology of Disease* **141**, 104954 (2020).

606 42. M. F. Schneider, M. Vogt, J. Scheuermann, V. Müller, A. H. L. Fischer-Hentrich, T. Kremer, S. Lugert, F.
607 Metzger, M. Kudernatsch, G. Kluger, T. Hartlieb, S. Noachtar, C. Vollmar, M. Kunz, J. C. Tonn, R. Coras, I.
608 Blümcke, C. Pace, F. Heinen, C. Klein, H. Potschka, I. Borggraefe, Brain expression profiles of two SCN1A
609 antisense RNAs in children and adolescents with epilepsy. *Transl Neurosci* **15**, 20220330 (2024).

610 43. J. Antinao Diaz, E. Chilcott, A. Almacellas Barbanoj, A. Keegan, A. McTague, J. H. Cross, S. Schorge, G.
611 Lignani, S. N. Waddington, R. Karda, AAV9-mediated targeting of natural antisense transcript as a novel treatment
612 for Dravet Syndrome. *bioRxiv* , 2024.09.27.615323 (2024).

613 44. Z. Han, C. Chen, A. Christiansen, S. Ji, Q. Lin, C. Anumonwo, C. Liu, S. C. Leiser, Meena, I. Aznarez, G. Liau,
614 L. L. Isom, Antisense oligonucleotides increase *Scn1a* expression and reduce seizures and SUDEP incidence in a
615 mouse model of Dravet syndrome. *Sci. Transl. Med.* **12**, eaaz6100 (2020).

616 45. Encoded Therapeutics Announces US IND Clearance and Australian CTA Approval for Dravet Syndrome Gene
617 Therapy Candidate ETX101*Encoded Therapeutics, Inc.* (available at https://encoded.com/press-releases/encoded-
618 therapeutics-announces-us-ind-clearance-and-australian-cta-approval-for-dravet-syndrome-gene-therapy-candidate-
619 etx101/).

620 46. Z. Liu, O. Chen, J. B. J. Wall, M. Zheng, Y. Zhou, L. Wang, H. Ruth Vaseghi, L. Qian, J. Liu, Systematic
621 comparison of 2A peptides for cloning multi-genes in a polycistronic vector. *Sci Rep* **7**, 2193 (2017).

622 47. X. Xiao, J. Li, R. J. Samulski, Production of high-titer recombinant adeno-associated virus vectors in the absence
623 of helper adenovirus. *J Virol* **72**, 2224–2232 (1998).

624 48. J.-Y. Kim, S. D. Grunke, Y. Levites, T. E. Golde, J. L. Jankowsky, Intracerebroventricular Viral Injection of the
625 Neonatal Mouse Brain for Persistent and Widespread Neuronal Transduction. *Journal of Visualized Experiments*
626 *(JoVE)* , e51863 (2014).

627 49. S. E. Gombash Lampe, B. K. Kaspar, K. D. Foust, Intravenous Injections in Neonatal Mice. *J Vis Exp* , 52037
628 (2014).

629 50. M. I. Love, W. Huber, S. Anders, Moderated estimation of fold change and dispersion for RNA-seq data with
630 DESeq2. *Genome Biology* **15**, 550 (2014).

631 51. T. Wu, E. Hu, S. Xu, M. Chen, P. Guo, Z. Dai, T. Feng, L. Zhou, W. Tang, L. Zhan, X. Fu, S. Liu, X. Bo, G.
632 Yu, clusterProfiler 4.0: A universal enrichment tool for interpreting omics data. *The Innovation* **2**, 100141 (2021).

633

634 **Acknowledgments:** We would like to thank A. Rahim and J. Baruteau for the use of their Home
635 Office PPL. We would like to thank, R.Towns, M. Bandol, N. Foster, N. Marzouki and the staff
636 from Biological Services for their help with maintenance of the DS colony at University College
637 London. Figures 1A and 2A were created in BioRender. Antinao Diaz, J. (2025)
638 https://BioRender.com/k81r069.

639

640 **Funding:** This work was supported by Great Ormond Street Hospital Children Charity and
641 Dravet Syndrome UK Charity (V4720 and V4919 to R.K), Medical Research Council
642 Development Pathway Funding Scheme (MR/Z505201/1 to R.K), LifeArc (P2020-
643 0008 and P2023-0011 to R.K), Therapeutic Acceleration Support (TAS), UCL (to R.K),
644 GOSH/Spark Research Grant V4019 (to G.L.), Medical Research Council Programme Grant
645 (MR/V034758/1 to G.L. and S.S.), Epilepsy Research UK Emerging Leader Fellowship (F1701
646 to G.L.), Medical Research Council New Investigator Project Grant (MR/S011005/1 to G.L.).

647

648 **Author contributions:** Conceptualization: R.K and S.N.W. Methodology: R.K, M.M and
649 E.M.C. Investigation: R.K, E.M.C, J.F.A.D, A.K, Z.W, V.F, A.A.B, G.L. Visualization: R.K and
650 E.M.C. Funding acquisition: R.K, S.S, M.M, S.N.W and G.L. Project administration: R.K.
651 Writing – original draft: R.K and E.M.C. Writing – review & editing: all authors.

652 **Competing interests:** RK, EMC, MM are co-inventors on patent application "Therapy for
653 Dravet Syndrome". RK, SS & SNW have consultancy agreements with Rocket Pharma. G.L. and
654 S.S. have equity in a company that aims to bring epilepsy gene therapy to the clinic.

655

656 **Data and materials availability:** All data associated with this study are present in the paper in
657 Supplementary Material. Requests for data should be addressed to R.K.

658 **Figures**

659 **Fig. 1**. **Novel gRNAs increase in endogenous *Scn1a in vitro*.** (A) Schematic illustrating
660 mechanism of action of CIRTS to increase endogenous *Scn1a* expression through targeting of
661 the lncRNA. (B) Schematic diagram of the AAV-CIRTS-gRNA construct. (C) 4 novel AAV-
662 CIRTS-gRNA constructs significantly increased endogenous *Scn1a* mRNA after transient
663 transfection of differentiated mouse Neuro2a cells. The homology of these gRNAs to the human
664 *SCN1ANAT* sequence are indicated on the graph as a %, with gRNAs ranked from least to most
665 homologous. One-way ANOVA with Dunnett's multiple comparisons.

666

667 **Fig. 2. Neonatal AAV-F-CIRTS-gRNA9 RNA editing *in vivo* increases survival of *Scn1a*$^{+/-}$**
668 **DS mice.** *Scn1a*$^{+/-}$ mice were administered either AAV-F-CIRTS-gRNA9 ($7x10^{10}$ vg/pup) or
669 AAV9-CIRTS-gRNA9 ($7x10^{11}$ vg/pup) at P0 by intracerebroventricular (ICV) and intravenous
670 (IV) injection, with PBS-treated *Scn1a*$^{+/-}$ and *Scn1a*$^{+/+}$ littermate controls. (A) Experimental
671 timeline. (B) Kaplan-Meier survival curves of treated mice with percentage survival shown. Log-
672 rank (Mantel-Cox) test. (C) Weights of treated mice. One-way ANOVA with Dunnett's multiple
673 comparison. (D) Total distance read-outs from open field analyses at 4 different timepoints.
674 Two-way ANOVA with Dunnett's multiple comparisons.

675

676 **Fig. 3. Dosage study of AAV-F-CIRTS-gRNA9 in *Scn1a*$^{+/-}$ mice.** AAV-F-CIRTS-gRNA9 was
677 administered at 2 additional doses ($1.75x10^{10}$ and $1.75x10^{11}$ vg/pup) and was compared to the
678 original $7x10^{10}$ vg/pup cohort presented in Fig. 2. (A) Kaplan-Meier survival curves of treated

679 mice with percentage survival shown. Log-rank (Mantel-Cox) test. (B) Weights of treated mice.
680 AAV-F-CIRTS-gRNA9 $1.75x10^{11}$ vg/pup mice were significantly different from *Scn1a*$^{+/-}$ PBS
681 mice at P70 & P80-95 (P=0.0214-0.0451). Mixed-effects analysis with Geisser-Greenhouse
682 correction. (C) Total distance read-outs from open field analyses at 4 different timepoints. Two-
683 way ANOVA with Dunnett's multiple comparisons.

684

685 **Fig. 4. Reduction of seizure burden following AAV-F-CIRTS-gRNA9 treatment.** (A) Febrile
686 seizure probability curves. (B) Severity of observed seizures ranked by Racine scale. Fisher's
687 exact test. (C) Heatmap with coloured squares indicating seizure activity, monitored by EEG.
688 Crosses indicate the death of an animal during EEG recording. (D) Average seizure duration in
689 mice which presented with seizures, during EEG. Unpaired, two-tailed t-test.

690

691 **Fig. 5. Restoration of *Scn1a* gene expression in the cortex and heart of AAV-F-CIRTS-**
692 **gRNA9 treated *Scn1a*$^{+/-}$ mice.** *Scn1a* gene expression in the (A) cortex and (B) heart between
693 *Scn1a*$^{+/+}$ and *Scn1a*$^{+/-}$ mice (P20-100 tissues) treated with non-targeting AAV-F-CIRTS-
694 gRNAluc vector compared to AAV-F-CIRTS-gRNA9 *Scn1a*$^{+/-}$ mice. One-way ANOVA with
695 Dunnett's multiple comparisons. (C) Vector copy number analysis in P100 cortex, heart and
696 liver. Two-way ANOVA with Tukey's multiple comparisons.

697

698 **Fig. 6. AAV-F-CIRTS-gRNA9 does not lead to toxicity *in vivo*.** (A) Representative brain and
699 liver immunohistochemistry images. Scale bar = 100 μm. (B) Quantification of reactive
700 astrocytes (GFAP immunohistochemistry) in the brain of treated mice; CA1 = CA1 region of the

701 hippocampus, CA3 = CA3 region of the hippocampus, VPM = Ventral posteromedial nucleus of
702 the thalamus. Two-way ANOVA with Šídák's multiple comparisons. (C) Quantification of
703 macrophages (CD68 immunohistochemistry) in the liver of treated mice**.** One-way ANOVA with
704 Dunnett's multiple comparisons.

705

706 **Fig. 7. RNA-seq depicting differential gene expression following AAV-F-CIRTS-gRNA9**
707 **treatment.** *Scn1a*$^{+/-}$ cortical tissue analysed at P50. Comparison of AAV-F-CIRTS-gRNAluc
708 and AAV-F-CIRTS-gRNA9 mice. (A) Volcano plot showing the main differentially expressed
709 genes (DEGs). (B) Heatmap showing top up- and down-regulated genes per comparison,
710 presented as z-score, ranked by P value. Driver gene ontology (GO) term classification of the
711 molecular function of (C) down-regulated DEGs. No molecular function GO terms for up-
712 regulated genes were identified.

713

714 **Fig. S1. *In vitro* validation of AAV-CIRTS machinery.** AAV-CIRTS-gRNAluc significantly
715 down-regulated luciferase expression in HEK293T cells after transient co-transfection with
716 AAV-SFFV-*luciferase*-T2A-*eGFP* plasmid. Luciferase expression normalised to protein
717 concentration within lysate. Unpaired, two-tailed t-test.

718

719 **Fig. S2. Characterisation of untreated *Scn1a*$^{+/-}$ DS mice.** (A) Kaplan-Meier survival curves of
720 untreated mice over 100 days of development with percentage survival shown. Log-rank
721 (Mantel-Cox) test. (B) Weights of untreated mice. (C) Total distance and maximum speed read-
722 outs from open field analyses at 4 different timepoints. Two-way ANOVA with Dunnett's

723 multiple comparisons. (D) Induction of febrile seizures with temperature of seizure onset. (E)
724 *Scn1a* gene expression in 4 brain regions. Two-way ANOVA with Šídák's multiple comparisons
725 within each brain region. (F) Quantification of reactive astrogliosis (GFAP
726 immunohistochemistry) in the brain of untreated mice; CA1 = CA1 region of the hippocampus,
727 CA3 = CA3 region of the hippocampus, VPM = Ventral posteromedial nucleus of the thalamus.

728

729 **Fig. S3. RNA-Seq analysis of untreated *Scn1a*$^{+/-}$ DS mice.** *Scn1a*$^{+/+}$and *Scn1a*$^{+/-}$ cortical tissue
730 analysed at P50. (A) Volcano plot showing the main differentially expressed genes. (B) Heatmap
731 showing top 10 up- and down-regulated genes, presented as z-score, ranked by P value. (C)
732 Confirmation of *Scn1a* down-regulation in *Scn1a*$^{+/-}$ mice with normalised read count, (-
733 0.77Log2FC P=5.85x10^{-6}). (D) Driver gene ontology (GO) term classification of the molecular
734 function of up-regulated DEGs. No molecular function GO terms for down-regulated genes were
735 identified.

736 **Fig. S4. Increased biodistribution and transgene expression of AAV-F-CAG-GFP vector**
737 **compared to AAV9.** Wild-type C57BL/6J mice were administered either AAV-F-CAG-GFP
738 (1.9x10^{10} vg/pup) or AAV9- CAG-GFP (1.9x10^{10} vg/pup or 1.9x10^{11} vg/pup) at P0 by
739 intravenous (IV) injection, with uninjected littermate controls. (A) Experimental timeline. (B) *Ex*
740 *vivo* images of organs from injected mice. Scale bar = 2mm. (C) Quantification of vector copy
741 number in discreet brain regions and visceral organs. One-way ANOVA with Dunnett's multiple
742 comparisons.

743

744 **Fig. S5. GFP biodistribution in the brain of AAV-F and AAV9-CAF-GFP vectors.**
745 Immunofluorescence stain showing GFP positive cells in the olfactory bulb (OFB), cortex,
746 hippocampus and cerebellum. Scale bar shown on the images.

747 **Fig. S6. Co-localisation and quantification of neuron and astrocyte targeting of AAV-F. (A)**
748 Representative images co-localisation of GFP and NeuN. Images were taken at 400X
749 magnification. Scale bar, 100µm. **(B)** Quantification of GFP and NeuN positive cells. One-way
750 ANOVA with Dunnett's multiple comparisons. **(C)** Representative images co-localisation of
751 GFP and GFAP. Images were taken at 400X magnification. Scale bar = 100µm. **(D)**
752 Quantification of GFP and GFAP positive cells. One-way ANOVA with Dunnett's multiple
753 comparisons.

754

755 **Fig. S7. Maximum speed of AAV-F/9-CIRTS-gRNA9 mice and survival curve for AAV-F-**
756 **CIRTS-gRNA9.** (A) Open field maximum speed assessment at 4 different timepoints. Two-way
757 ANOVA with Dunnett's multiple comparisons. (B) Kaplan-Meier survival curves of treated mice
758 with percentage survival shown. Log-rank (Mantel-Cox) test.

759

760 **Fig. S8. Neonatal AAV-F/9-CIRTS- gRNA21 treatment.** *Scn1a*$^{+/-}$ mice were administered
761 either AAV-F-CIRTS-gRNA21 at 7x10^{10} vg/pup or AAV-9-CIRTS-gRNA21 at 7x10^{11} vg/pup,
762 with PBS-treated *Scn1a*$^{+/-}$ and *Scn1a*$^{+/+}$ littermate controls. (A) Kaplan-Meier survival curves of
763 treated mice with percentage survival shown. Log-rank (Mantel-Cox) test. (B) Weights of treated
764 mice. AAV-9-CIRTS-gRNA21 was significantly different from *Scn1a*$^{+/-}$ PBS mice at P90 only
765 (P=0.0390), but only female mice were alive in the treatment group at this time (100% female at

766 P100 vs 25% female in *Scn1a*$^{+/-}$ PBS). Mixed-effects analysis with Geisser-Greenhouse
767 correction. (C) Total distance and (D) maximum speed read-outs from open field analyses at 4
768 different timepoints. Two-way ANOVA with Dunnett's multiple comparisons.

769

770 **Fig. S9. Maximum speed of AAV-F-CIRTS-gRNA9 dosage.** 4 different timepoints. Two-way
771 ANOVA with Dunnett's multiple comparisons.

772

773 **Fig. S10. Seizure monitoring in AAV-F-CIRTS-gRNA9 treated DS mice.** (A) Total seizures
774 measured in 15 days. Mann-Whitney test. (B) Average number of seizures per day. Unpaired,
775 two tailed t-test (C) Cumulative seizure duration. Unpaired, two tailed t-test.

776

777 **Fig. S11. *YTHDF2* gene expression analysis.** P100 cortex, heart and liver. Two-way ANOVA
778 with Tukey's multiple comparisons.

779

780 **Fig. S12. AAV-F-CIRTS-gRNA9/luc administration to healthy mice.** *Scn1a*$^{+/+}$ mice were
781 administered either AAV-F-CIRTS-gRNA9 or AAV-F-CIRTS-gRNAluc at the optimum
782 therapeutic dose $7x10^{10}$ vg/pup, or 1 dose higher at $1.75x10^{11}$ vg/pup to assess signs of toxicity,
783 compared to PBS littermates. (A) Kaplan-Meier survival curves of treated mice with percentage
784 survival shown. Log-rank (Mantel-Cox) test. (B) Weights of treated mice. One-way ANOVA
785 with Dunnett's multiple comparison. (C) Total distance and (D) maximum speed read-outs from
786 open field analyses at 4 different timepoints. Two-way ANOVA with Dunnett's multiple
787 comparisons.

Figure 1

A

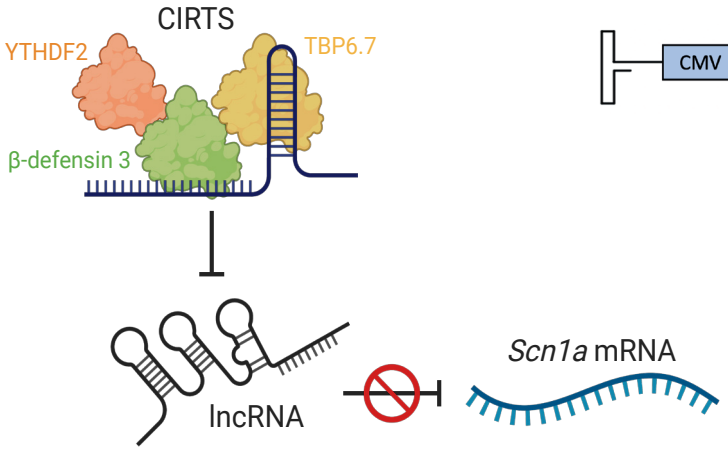
CIRTS
YTHDF2
TBP6.7
β-defensin 3
lncRNA
Scn1a mRNA

B

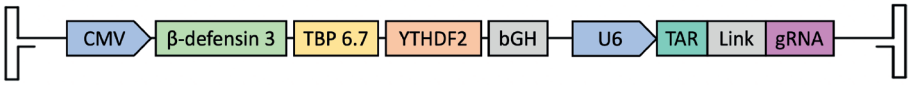
CMV
β-defensin 3
TBP 6.7
YTHDF2
bGH
U6
TAR
Link
gRNA

C

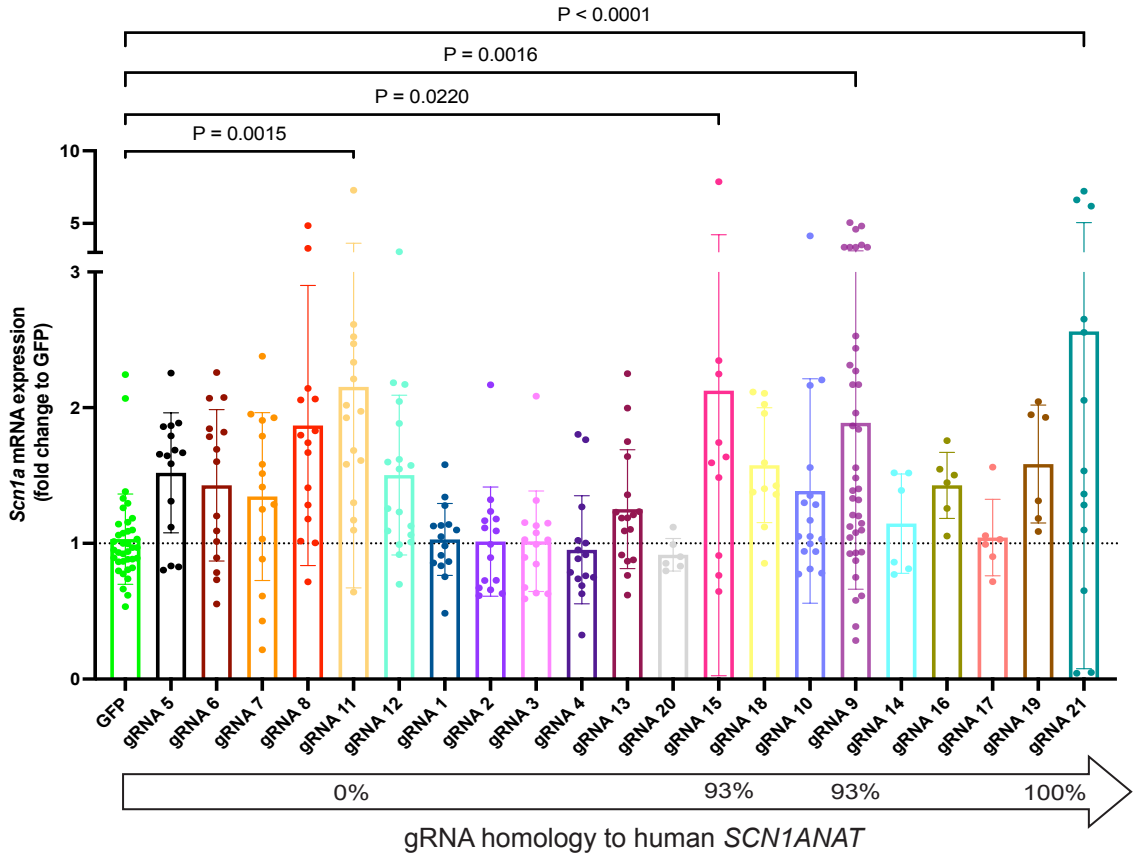
P < 0.0001
P = 0.0016
P = 0.0220
P = 0.0015
Scn1a mRNA expression (fold change to GFP)
GFP
gRNA 5
gRNA 6
gRNA 7
gRNA 8
gRNA 11
gRNA 12
gRNA 1
gRNA 2
gRNA 3
gRNA 4
gRNA 13
gRNA 20
gRNA 15
gRNA 18
gRNA 10
gRNA 9
gRNA 14
gRNA 16
gRNA 17
gRNA 19
gRNA 21
0%
93%
93%
100%
gRNA homology to human SCN1ANAT

Figure 2

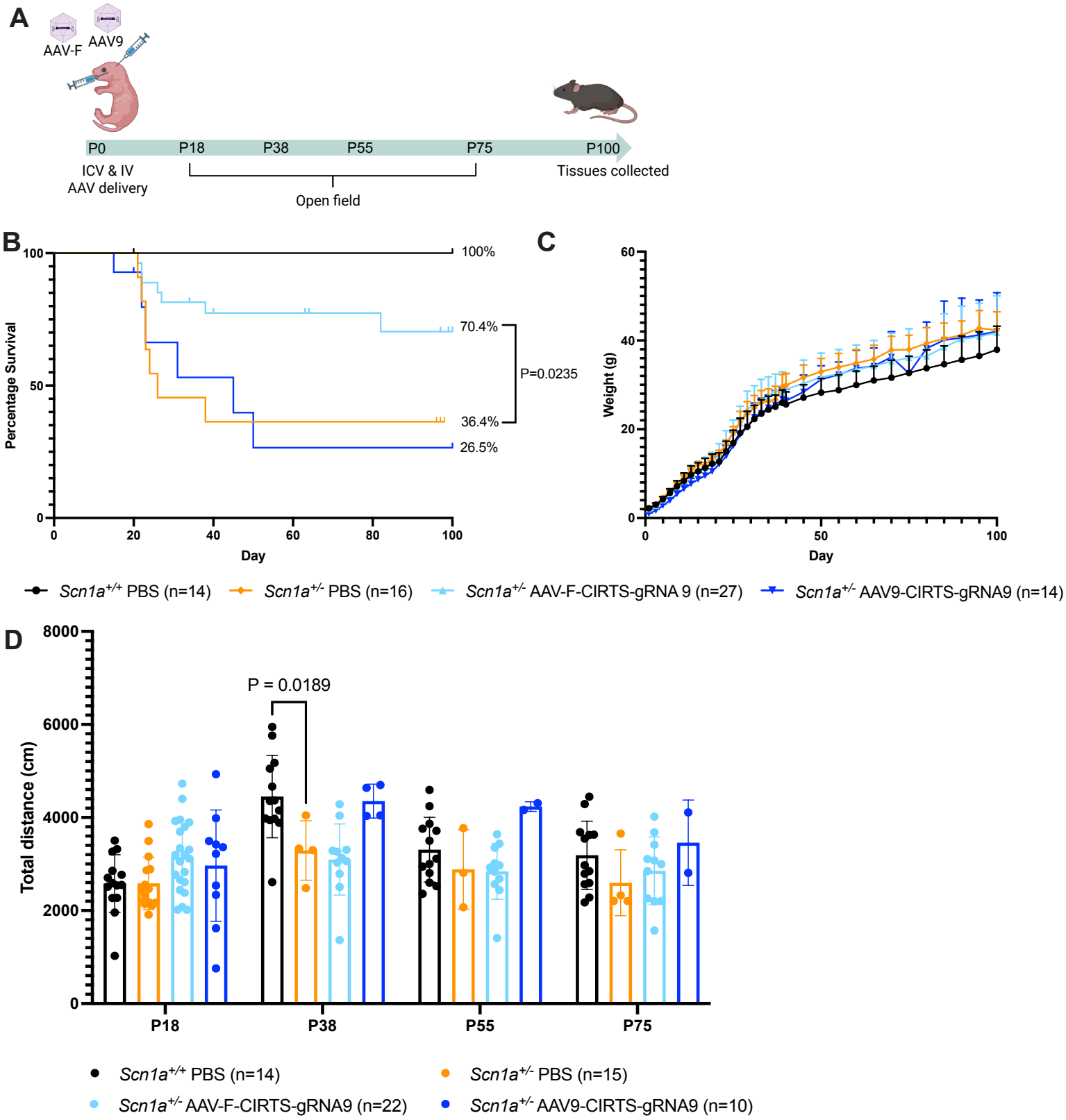
A
AAV-F
AAV9
P0
P18
P38
P55
P75
P100
ICV & IV
AAV delivery
Open field
Tissues collected
B
Percentage Survival
Day
100%
70.4%
36.4%
26.5%
P=0.0235
C
Weight (g)
Day
Scn1a+/+ PBS (n=14)
Scn1a+/- PBS (n=16)
Scn1a+/- AAV-F-CIRTS-gRNA 9 (n=27)
Scn1a+/- AAV9-CIRTS-gRNA9 (n=14)
D
Total distance (cm)
P = 0.0189
P18
P38
P55
P75
Scn1a+/+ PBS (n=14)
Scn1a+/- PBS (n=15)
Scn1a+/- AAV-F-CIRTS-gRNA9 (n=22)
Scn1a+/- AAV9-CIRTS-gRNA9 (n=10)

Figure 3

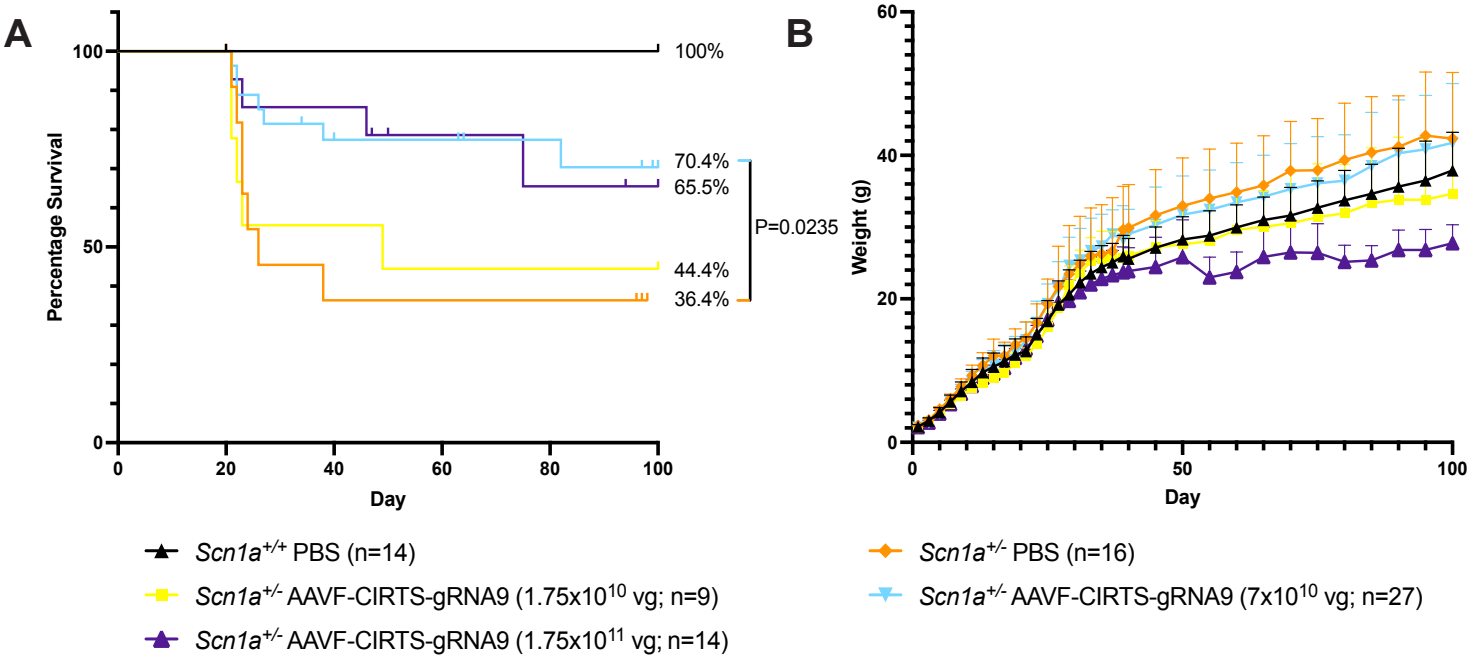
A
Percentage Survival
Day
100%
70.4%
65.5%
44.4%
36.4%
P=0.0235
B
Weight (g)
Day
Scn1a+/+ PBS (n=14)
Scn1a+/- AAVF-CIRTS-gRNA9 (1.75x10^10 vg; n=9)
Scn1a+/- AAVF-CIRTS-gRNA9 (1.75x10^11 vg; n=14)
Scn1a+/- PBS (n=16)
Scn1a+/- AAVF-CIRTS-gRNA9 (7x10^10 vg; n=27)

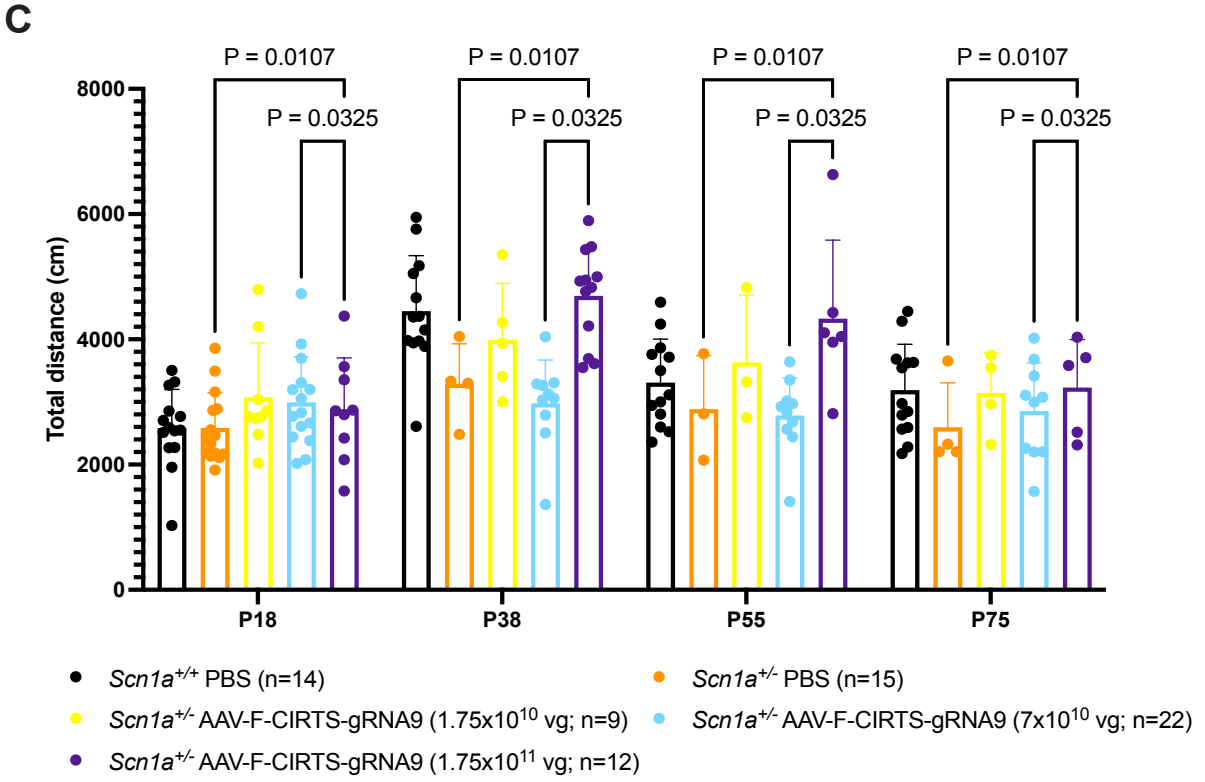
C
Total distance (cm)
P = 0.0107
P = 0.0325
P18
P38
P55
P75
Scn1a+/+ PBS (n=14)
Scn1a+/- PBS (n=15)
Scn1a+/- AAV-F-CIRTS-gRNA9 (1.75x10^10 vg; n=9)
Scn1a+/- AAV-F-CIRTS-gRNA9 (7x10^10 vg; n=22)
Scn1a+/- AAV-F-CIRTS-gRNA9 (1.75x10^11 vg; n=12)

Figure 4

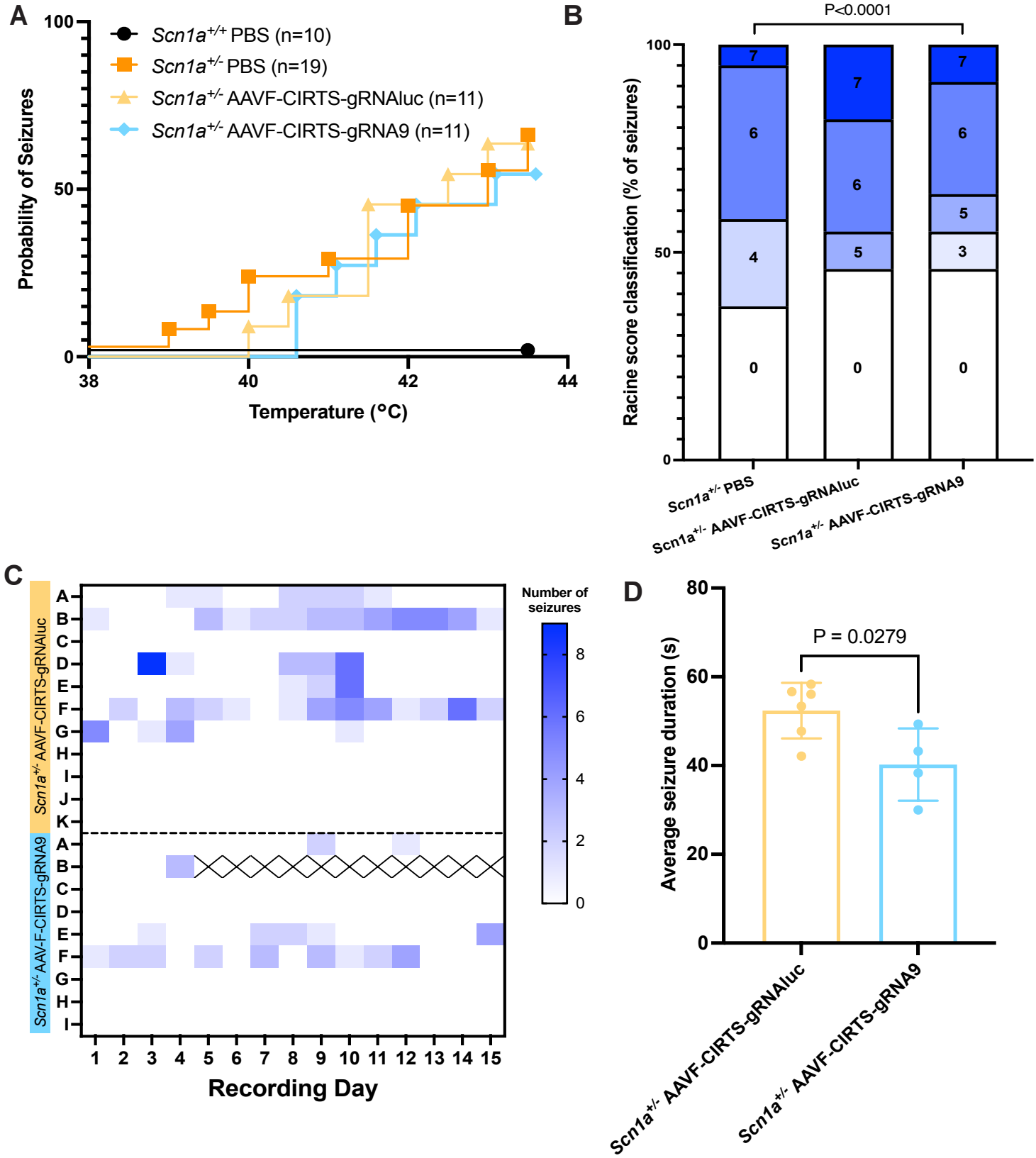
A
Probability of Seizures
Temperature (°C)
Scn1a+/+ PBS (n=10)
Scn1a+/- PBS (n=19)
Scn1a+/- AAVF-CIRTS-gRNAluc (n=11)
Scn1a+/- AAVF-CIRTS-gRNA9 (n=11)
B
Racine score classification (% of seizures)
P<0.0001
P=0.0111
P<0.0001
Scn1a+/- PBS
Scn1a+/- AAVF-CIRTS-gRNAluc
Scn1a+/- AAVF-CIRTS-gRNA9
C
Scn1a+/- AAVF-CIRTS-gRNAluc
Scn1a+/- AAV-F-CIRTS-gRNA9
Number of seizures
Recording Day
D
Average seizure duration (s)
P = 0.0279
Scn1a+/- AAVF-CIRTS-gRNAluc
Scn1a+/- AAVF-CIRTS-gRNA9

Figure 5

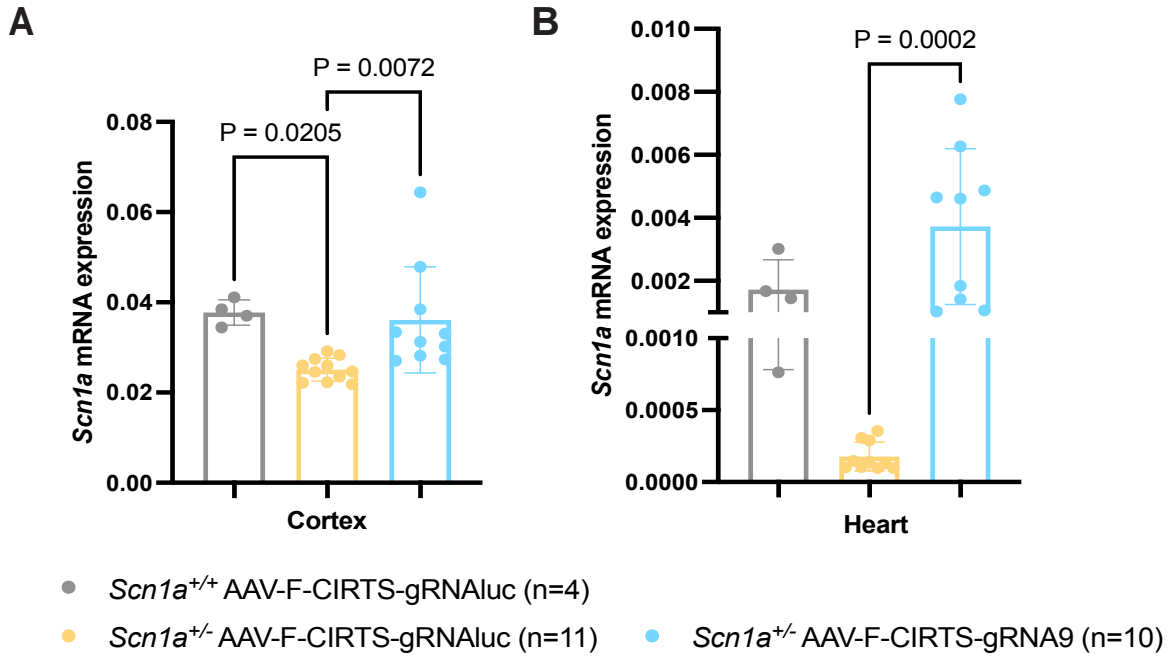
A
B
P = 0.0072
P = 0.0205
P = 0.0002
Scn1a mRNA expression
0.08
0.06
0.04
0.02
0.00
0.010
0.008
0.006
0.004
0.002
0.0010
0.0005
0.0000
Cortex
Heart
Scn1a+/+ AAV-F-CIRTS-gRNAluc (n=4)
Scn1a+/- AAV-F-CIRTS-gRNAluc (n=11)
Scn1a+/- AAV-F-CIRTS-gRNA9 (n=10)

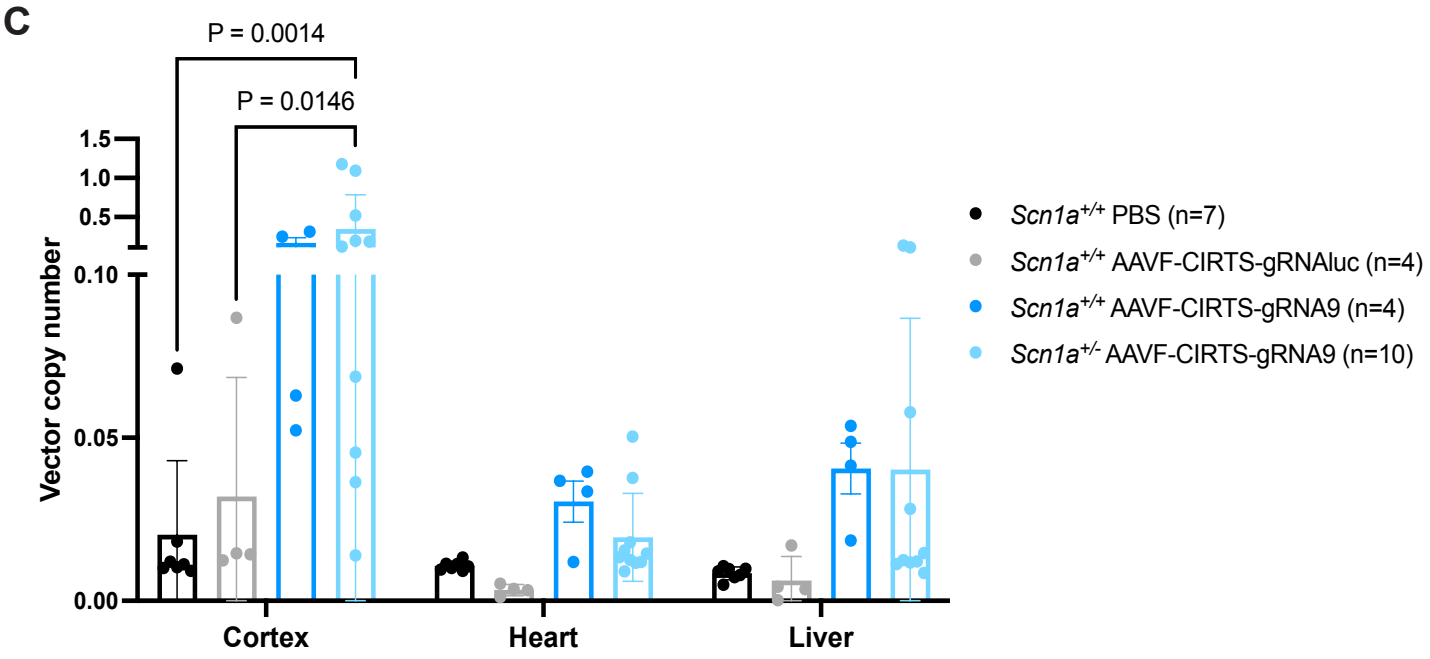
C
P = 0.0014
P = 0.0146
Vector copy number
1.5
1.0
0.5
0.10
0.05
0.00
Cortex
Heart
Liver
Scn1a+/+ PBS (n=7)
Scn1a+/+ AAVF-CIRTS-gRNAluc (n=4)
Scn1a+/+ AAVF-CIRTS-gRNA9 (n=4)
Scn1a+/- AAVF-CIRTS-gRNA9 (n=10)

Figure 6

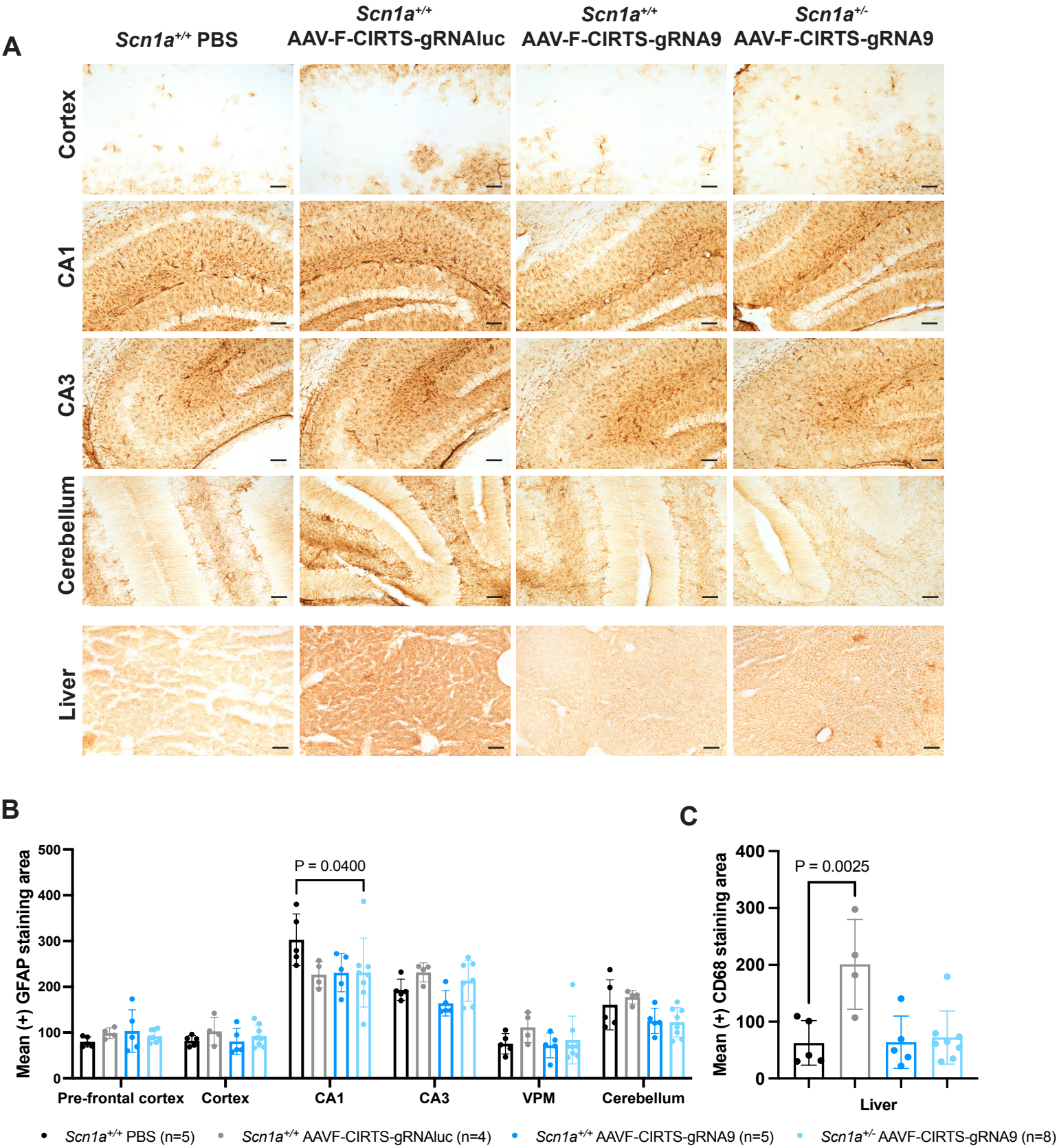
A
Scn1a+/+ PBS
Scn1a+/+ AAV-F-CIRTS-gRNAluc
Scn1a+/+ AAV-F-CIRTS-gRNA9
Scn1a+/- AAV-F-CIRTS-gRNA9
Cortex
CA1
CA3
Cerebellum
Liver
B
Mean (+) GFAP staining area
500
400
300
200
100
0
P = 0.0400
Pre-frontal cortex
Cortex
CA1
CA3
VPM
Cerebellum
C
Mean (+) CD68 staining area
400
300
200
100
0
P = 0.0025
Liver
Scn1a+/+ PBS (n=5)
Scn1a+/+ AAVF-CIRTS-gRNAluc (n=4)
Scn1a+/+ AAVF-CIRTS-gRNA9 (n=5)
Scn1a+/- AAVF-CIRTS-gRNA9 (n=8)

Figure 7

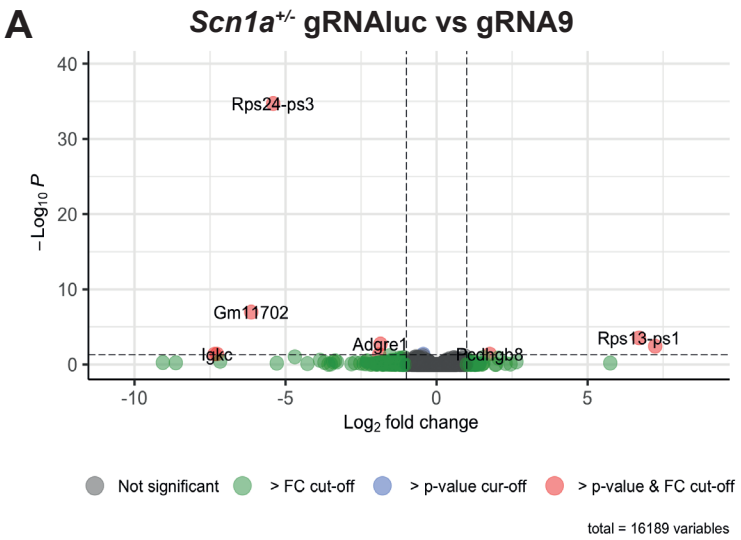
A
Scn1a+/- gRNAluc vs gRNA9
Rps24-ps3
Gm11702
Igkc
Adgre1
Pcdhgb8
Rps13-ps1
−Log10 P
Log2 fold change
Not significant
> FC cut-off
> p-value cur-off
> p-value & FC cut-off
total = 16189 variables

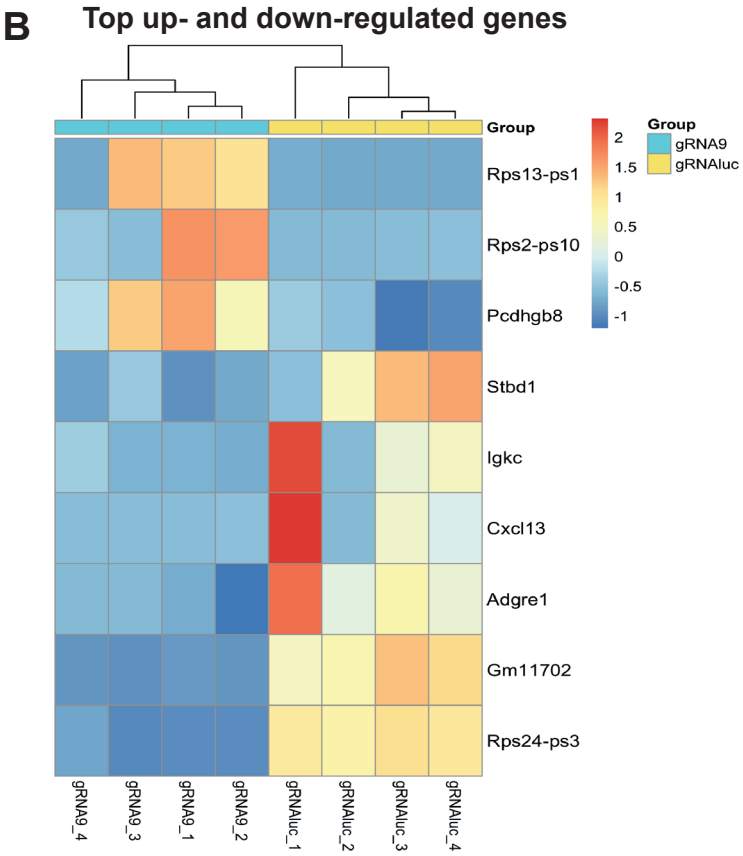
B
Top up- and down-regulated genes
Group
gRNA9
gRNAluc
Rps13-ps1
Rps2-ps10
Pcdhgb8
Stbd1
Igkc
Cxcl13
Adgre1
Gm11702
Rps24-ps3
gRNA9_4
gRNA9_3
gRNA9_1
gRNA9_2
gRNAluc_1
gRNAluc_2
gRNAluc_3
gRNAluc_4

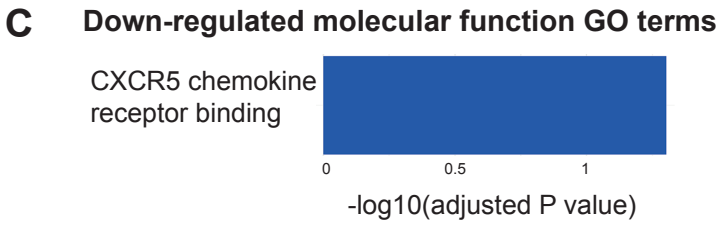
C
Down-regulated molecular function GO terms
CXCR5 chemokine receptor binding
-log10(adjusted P value)

Supplementary Figure 1

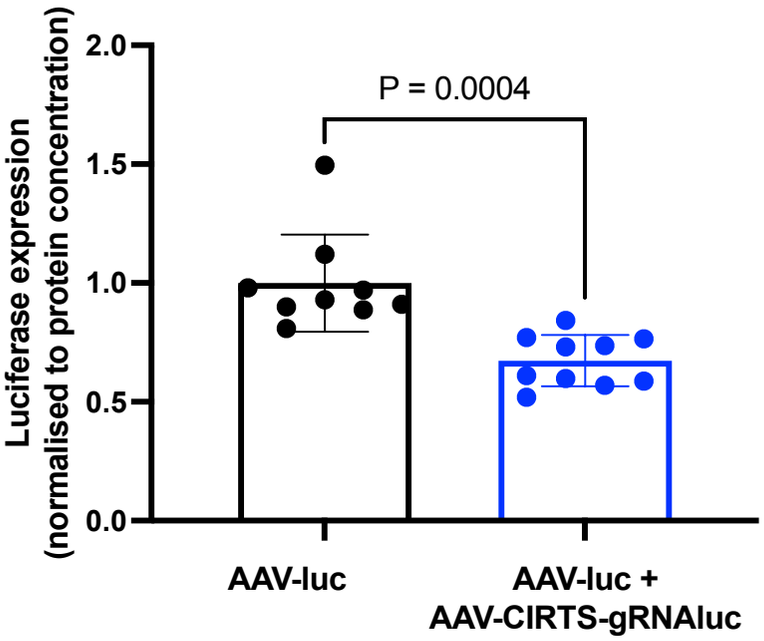

Supplementary Figure 2

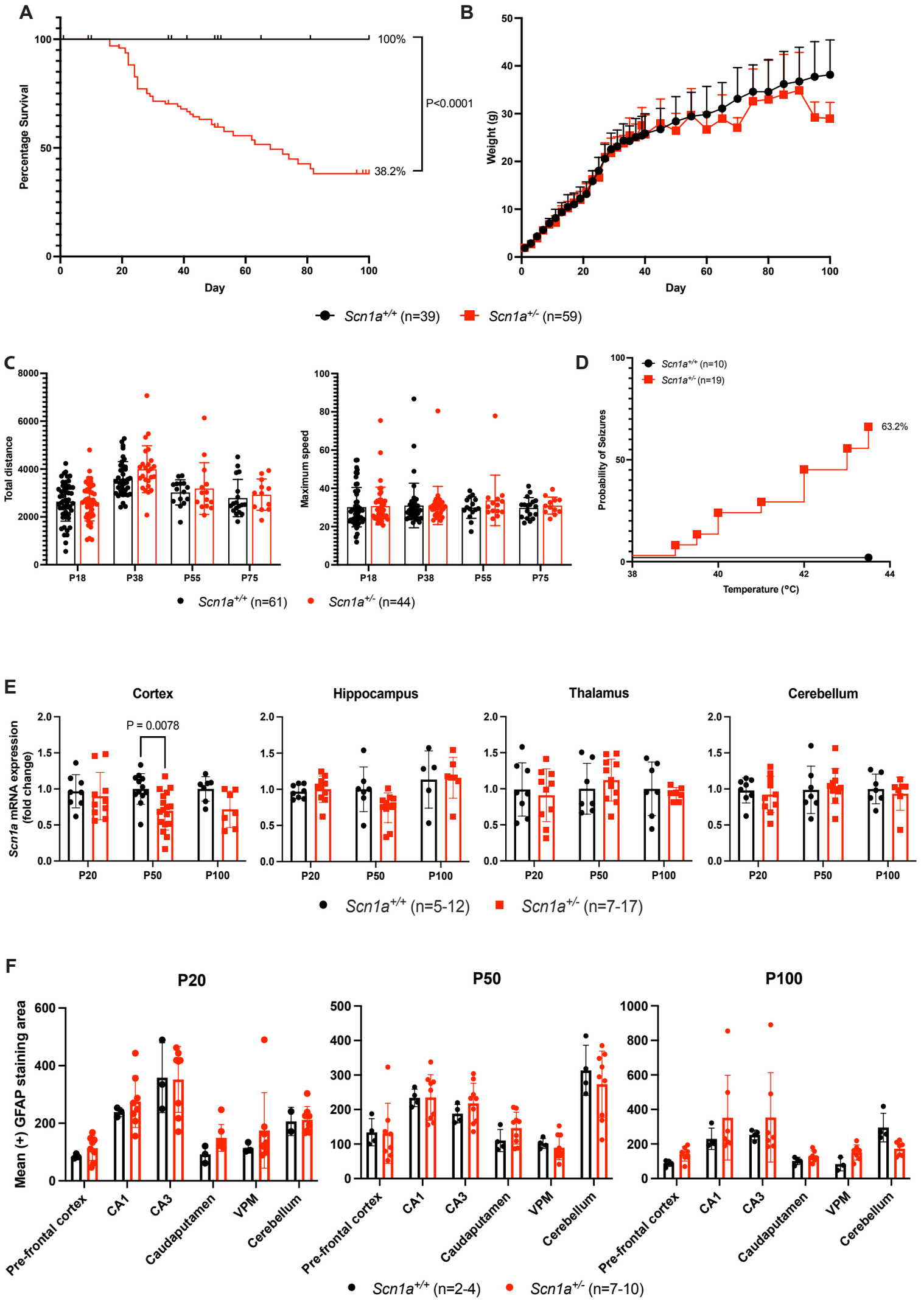

Supplementary Figure 3

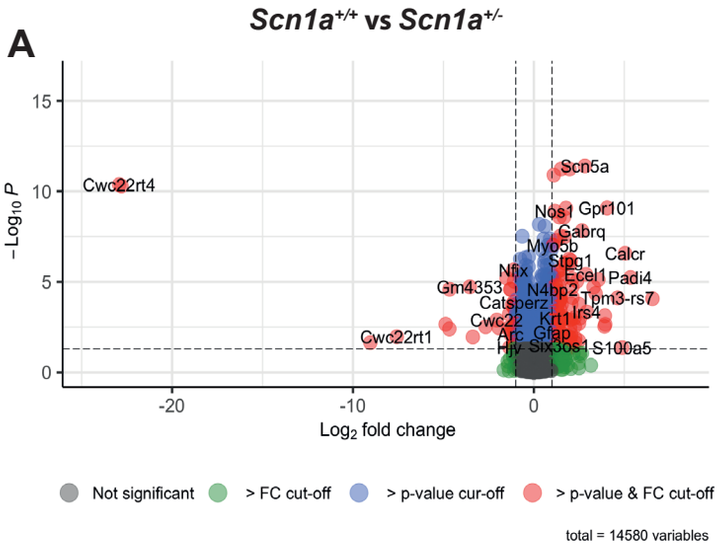

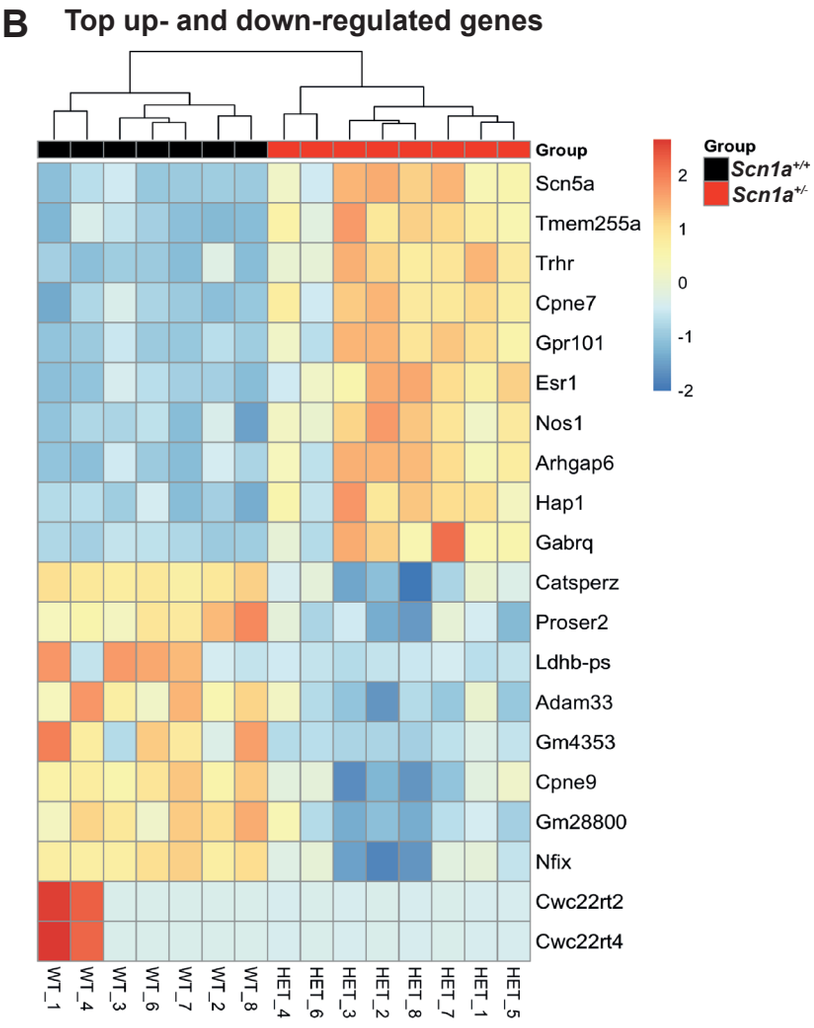

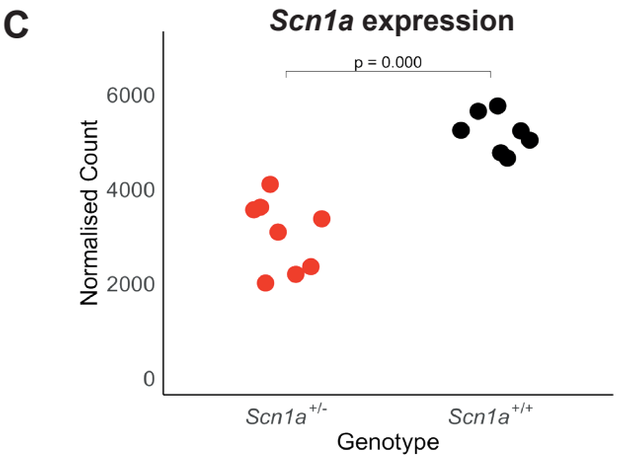

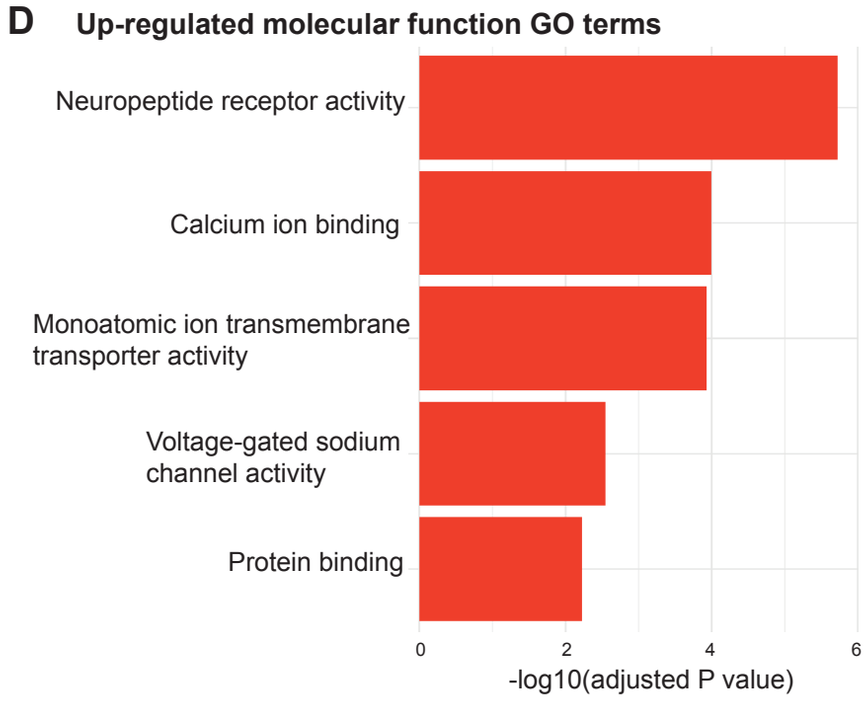

Supplementary Figure 4

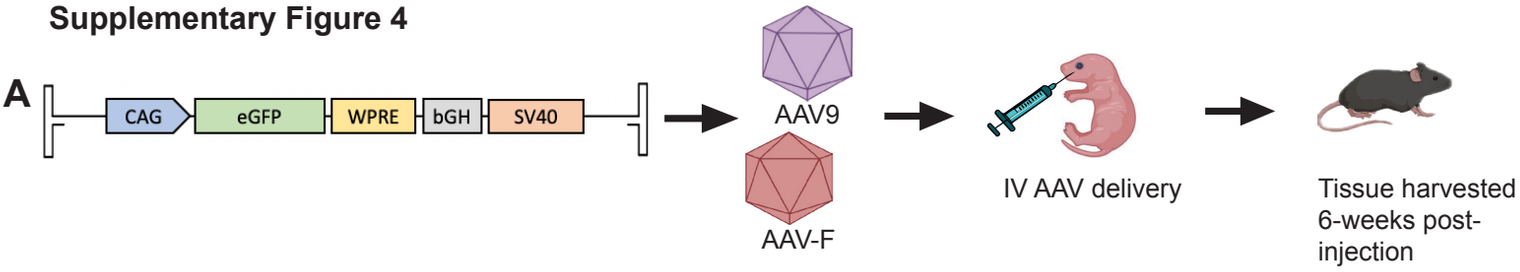

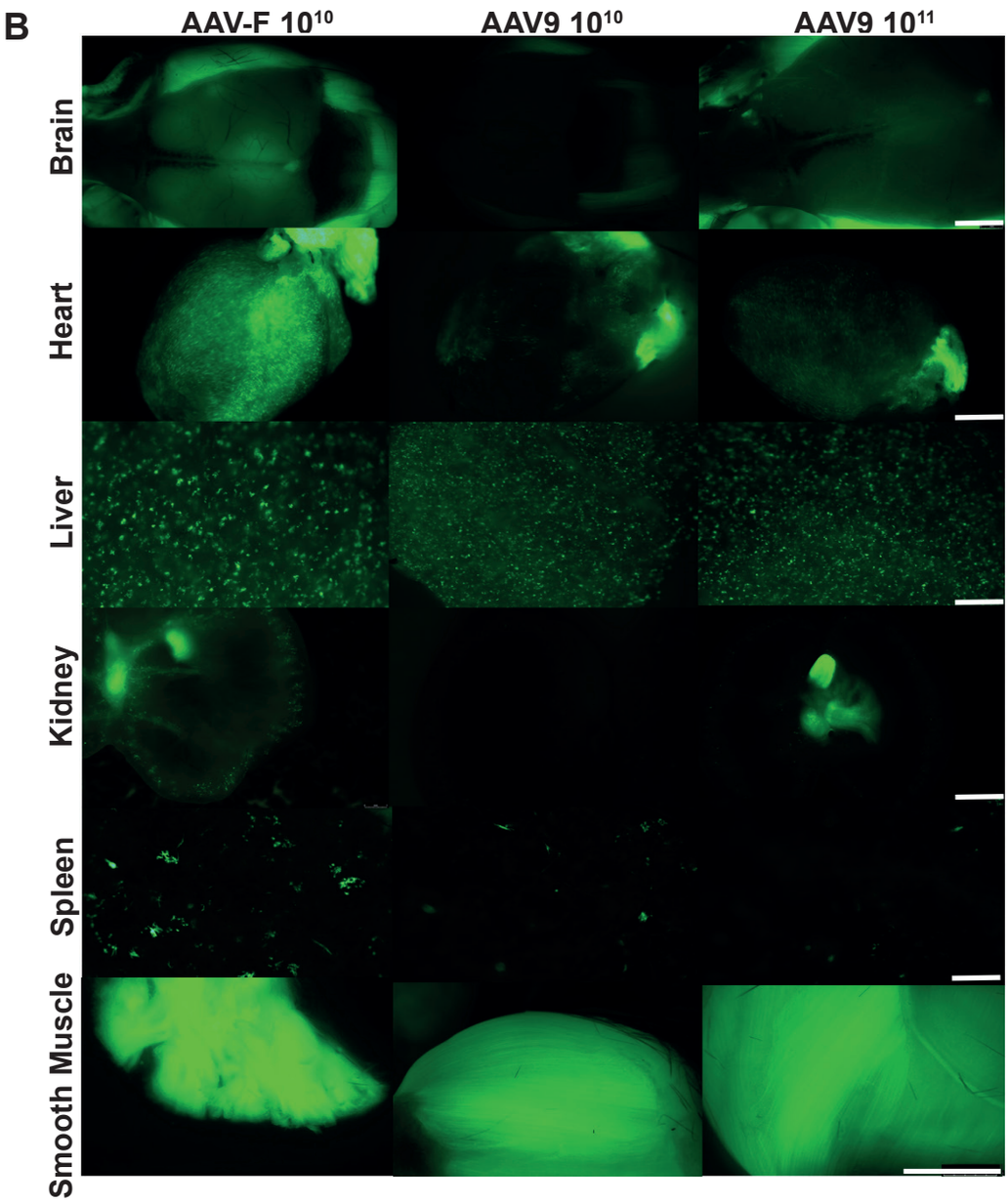

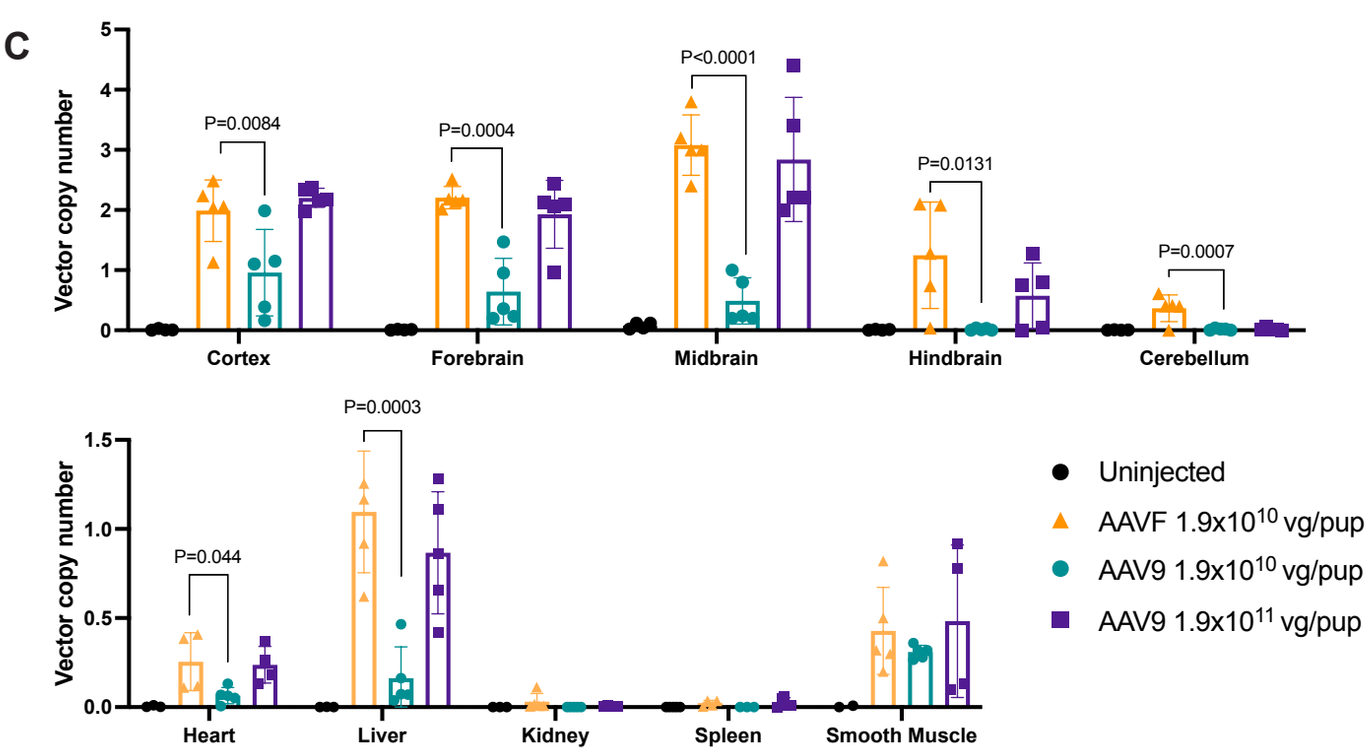

Supplementary Figure 5

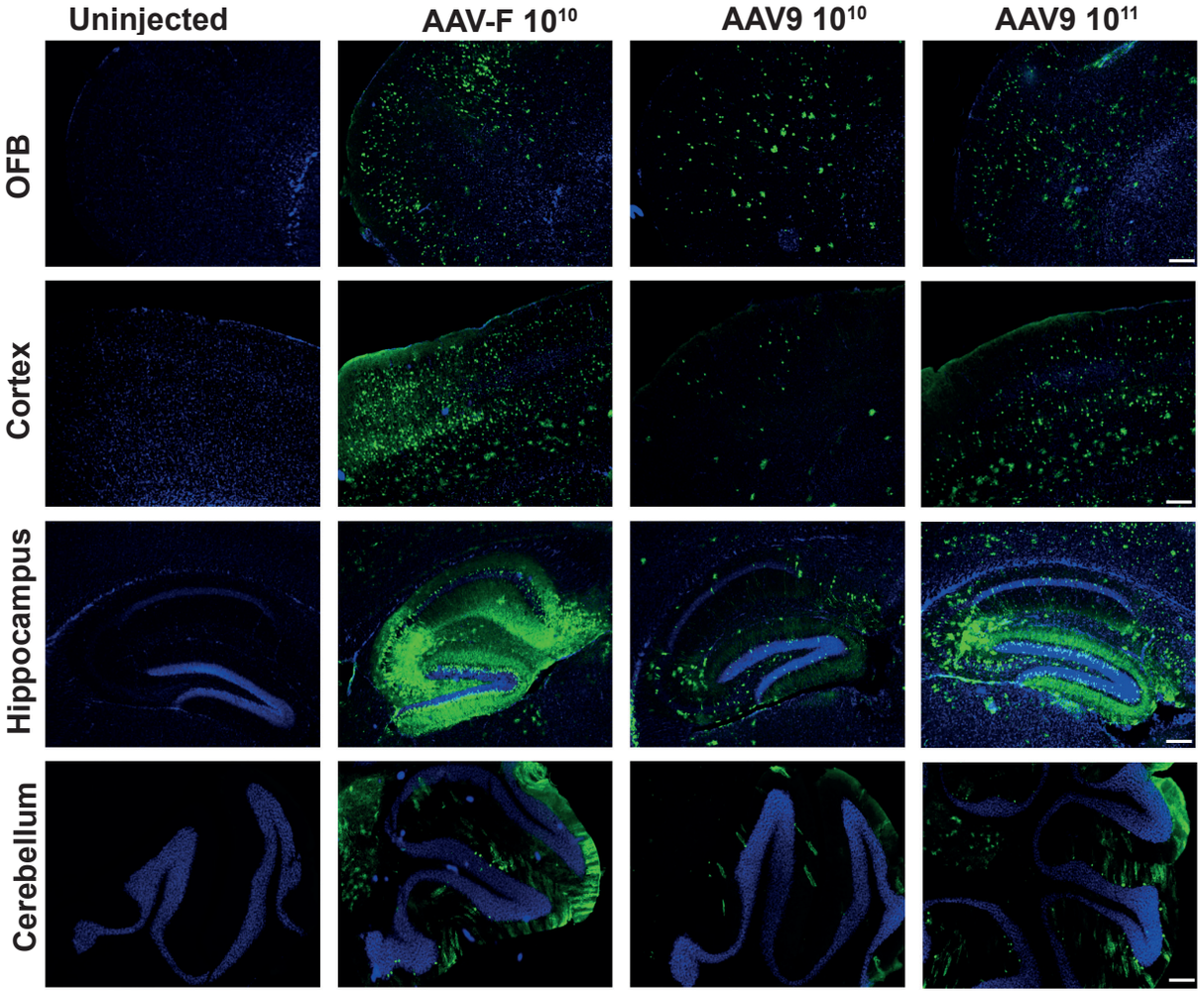

Supplementary Figure 6

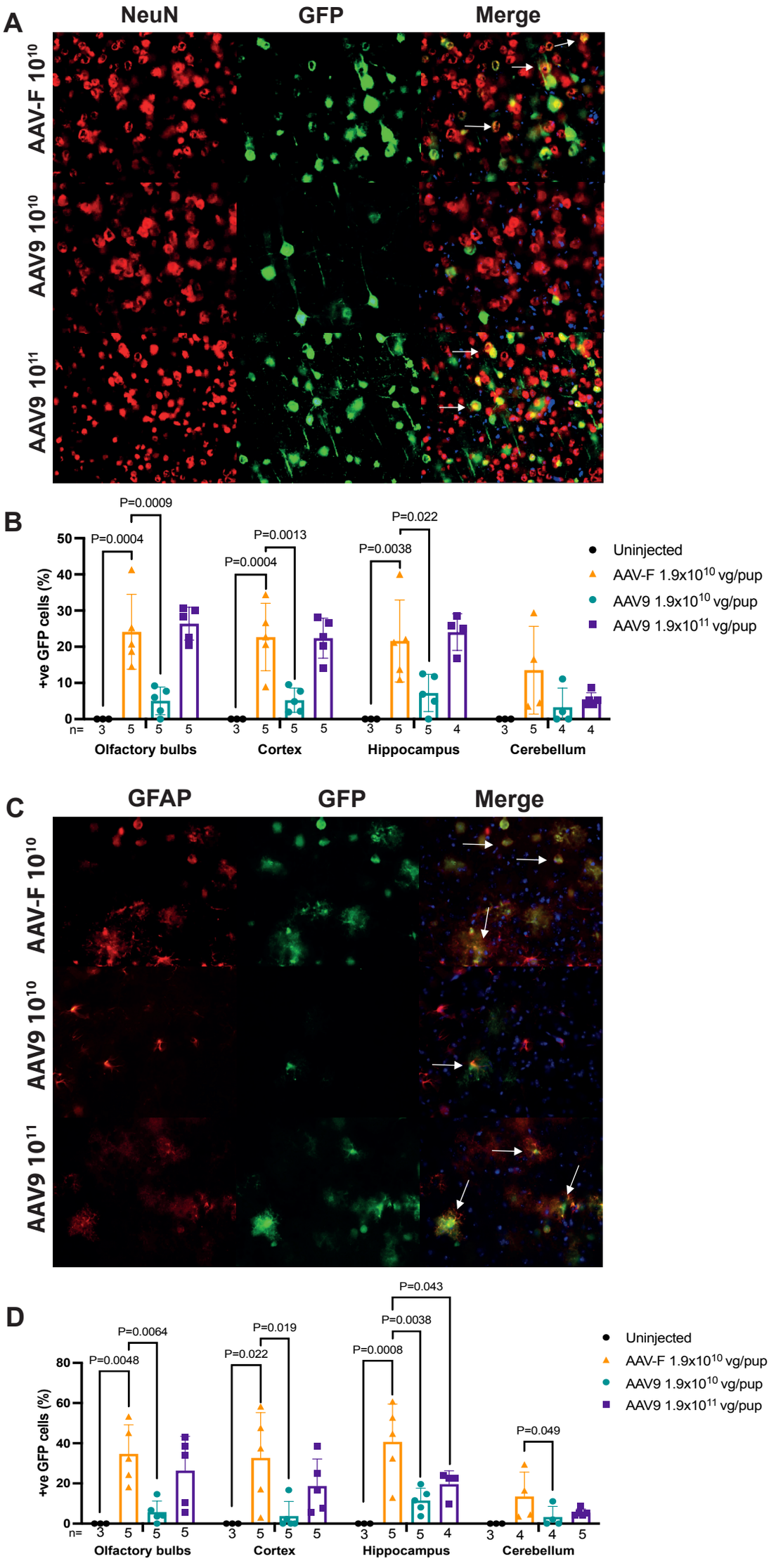

Supplementary Figure 7

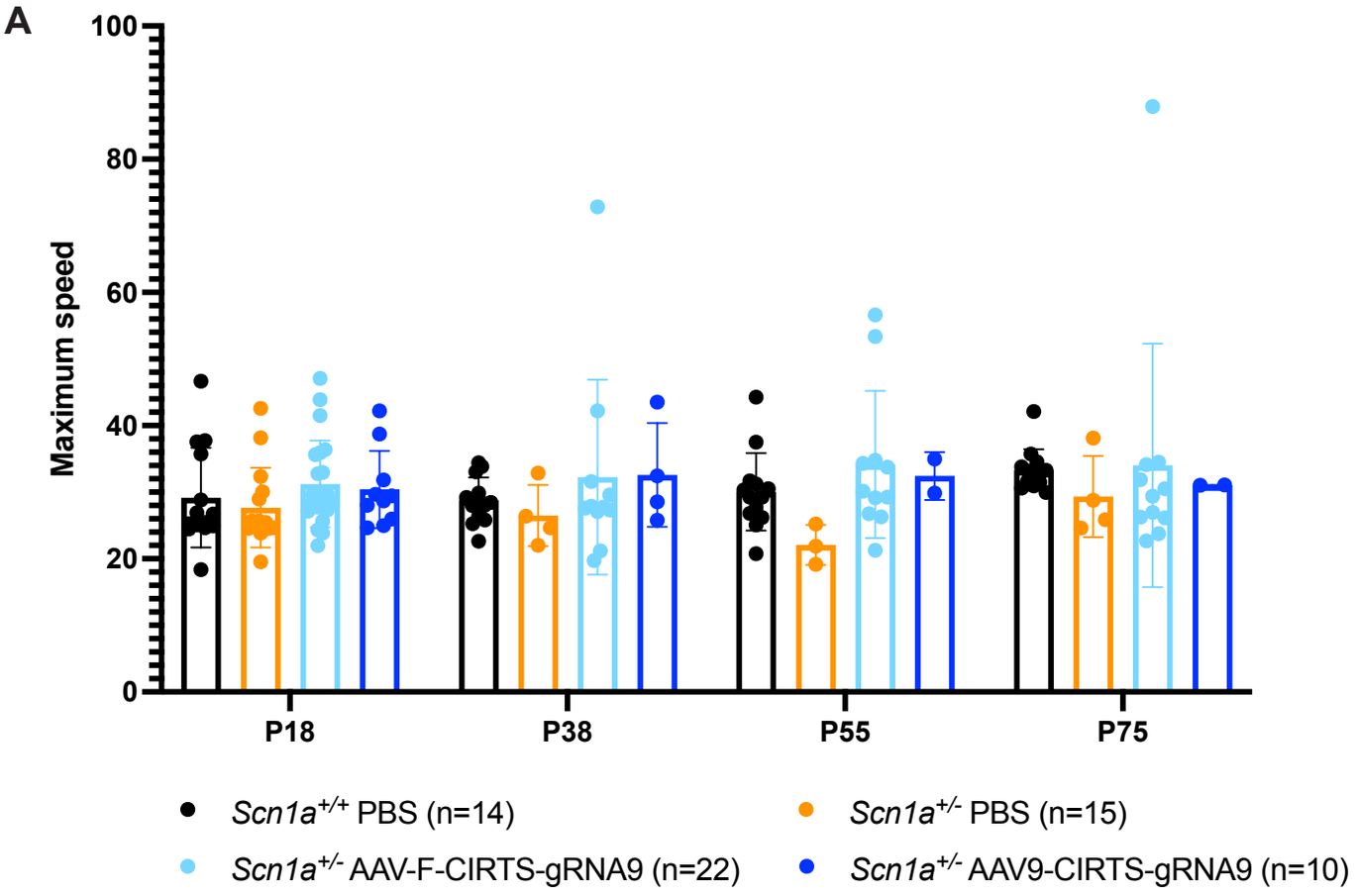

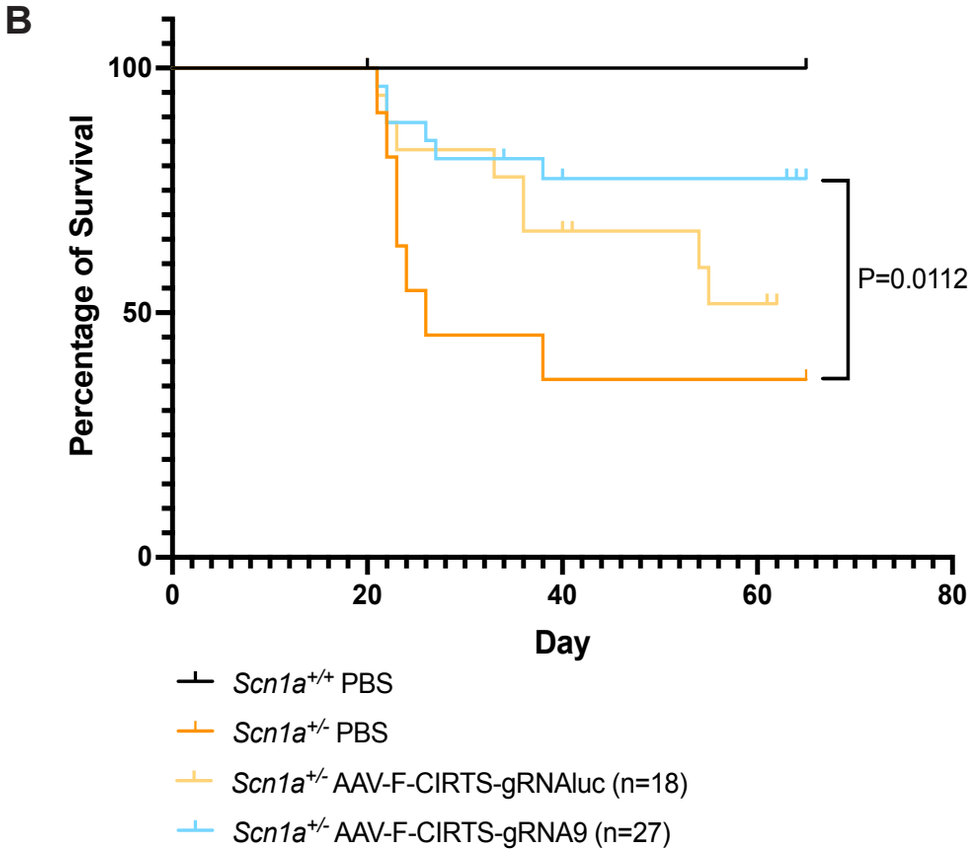

Supplementary Figure 8

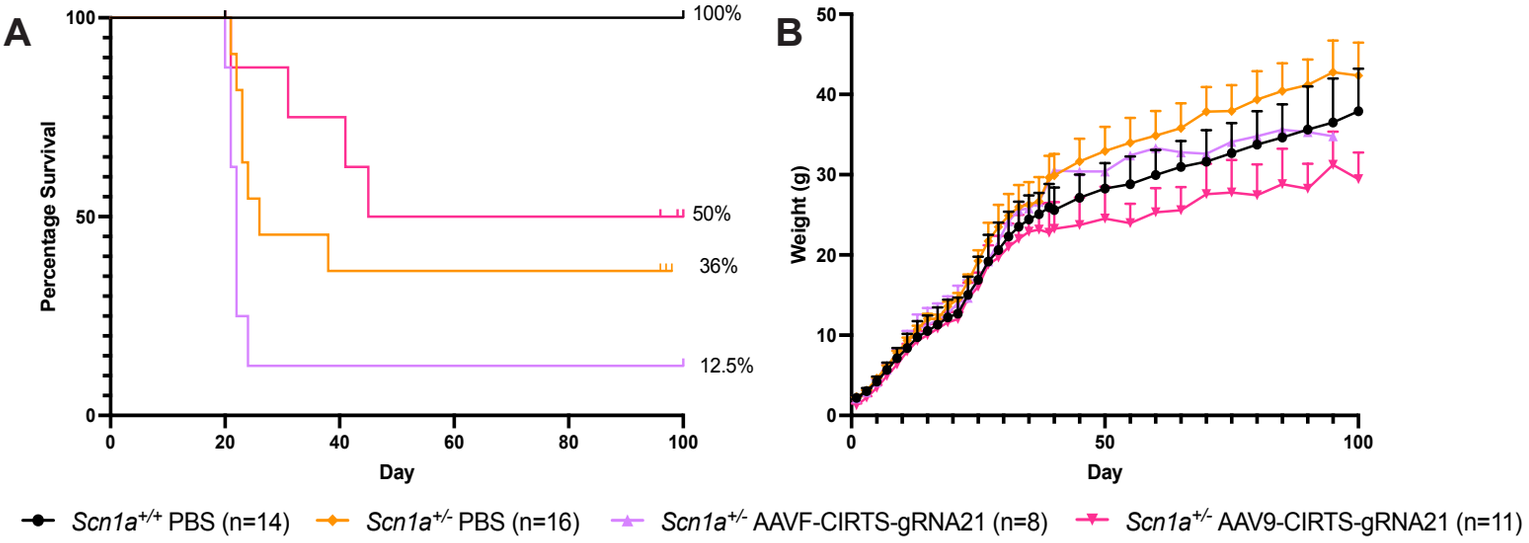

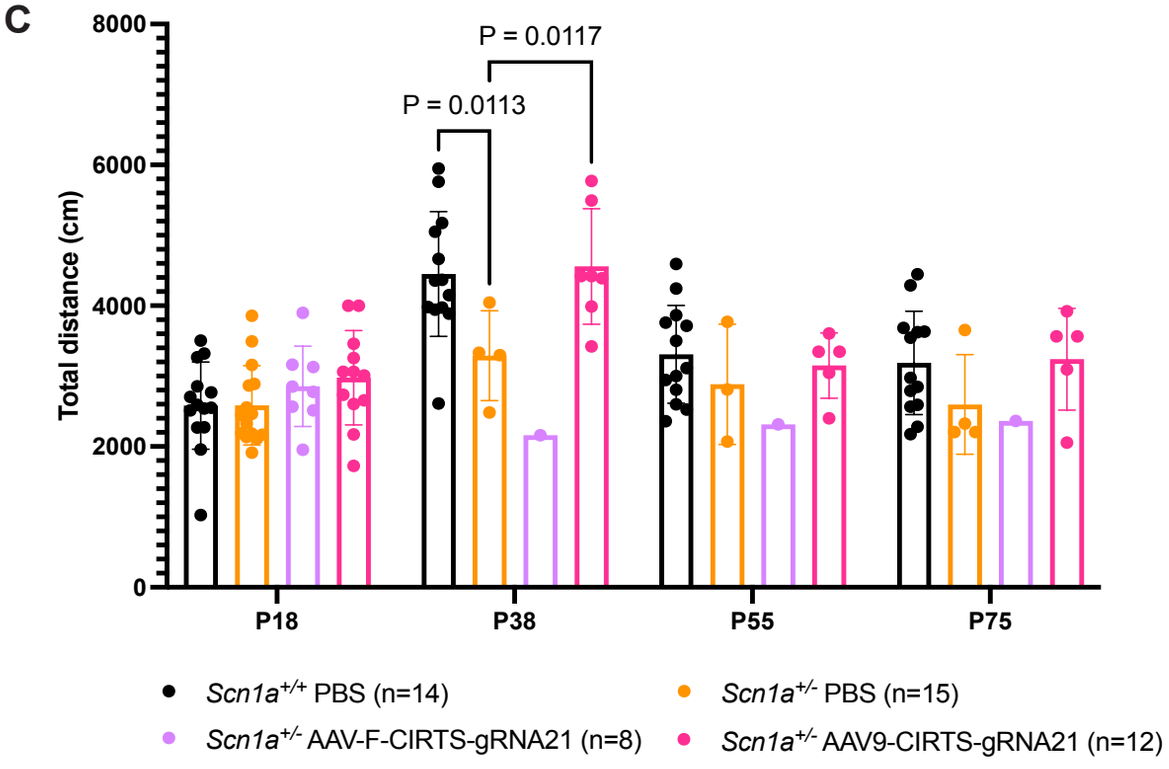

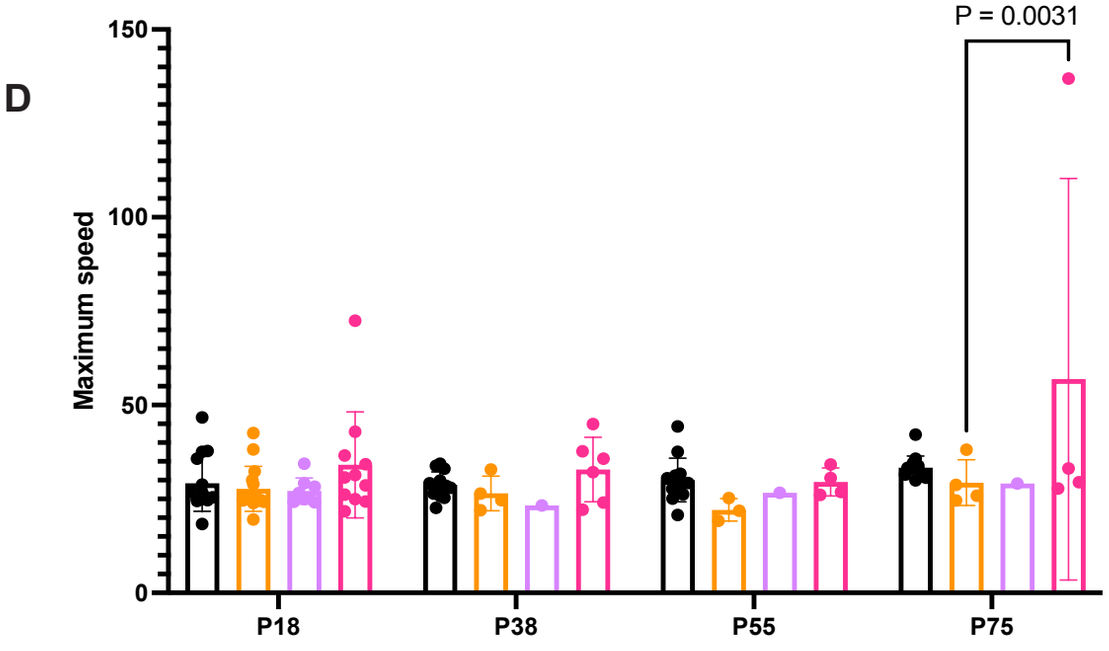

Supplementary Figure 9

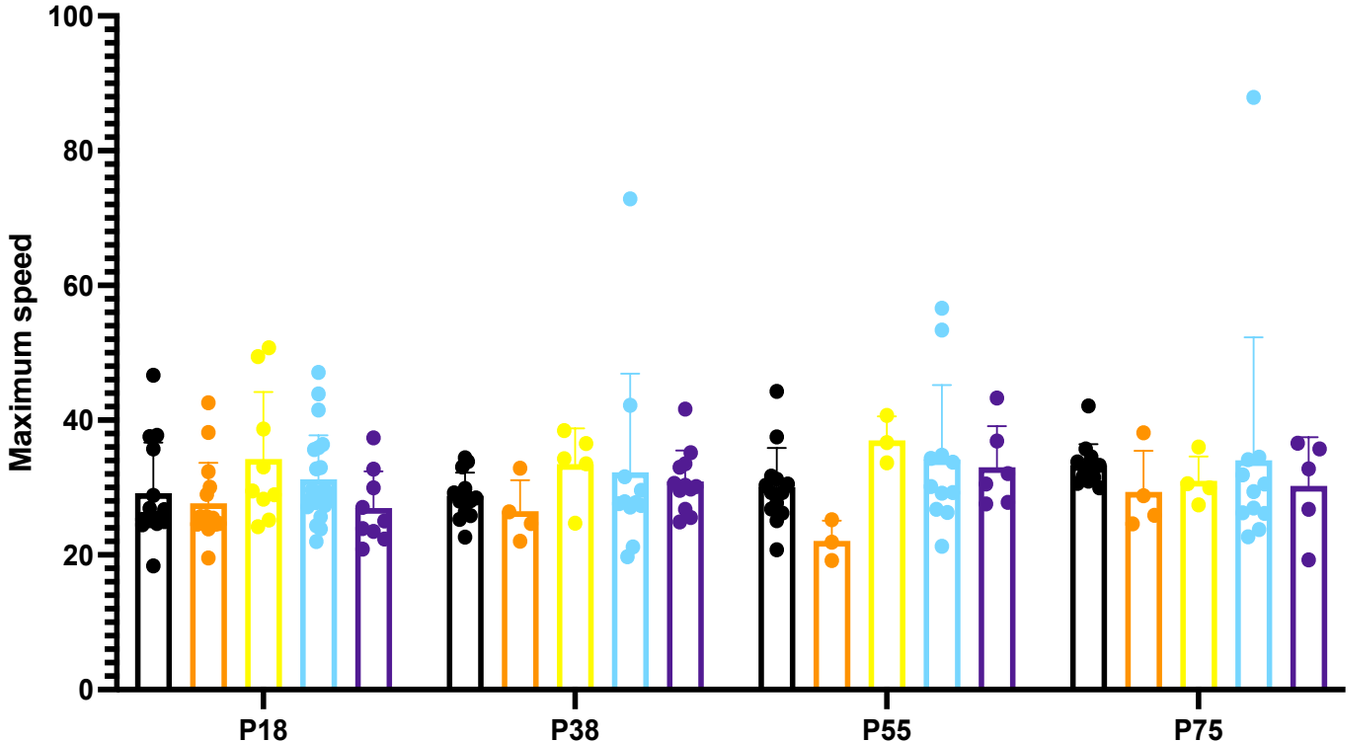

- *Scn1a*$^{+/+}$ PBS (n=14)
- *Scn1a*$^{+/-}$ PBS (n=15)
- *Scn1a*$^{+/-}$ AAV-F-CIRTS-gRNA9 (1.75x10^{10} vg; n=9)
- *Scn1a*$^{+/-}$ AAV-F-CIRTS-gRNA9 (7x10^{10} vg; n=22)
- *Scn1a*$^{+/-}$ AAV-F-CIRTS-gRNA9 (1.75x10^{11} vg; n=12)

Supplementary Figure 10

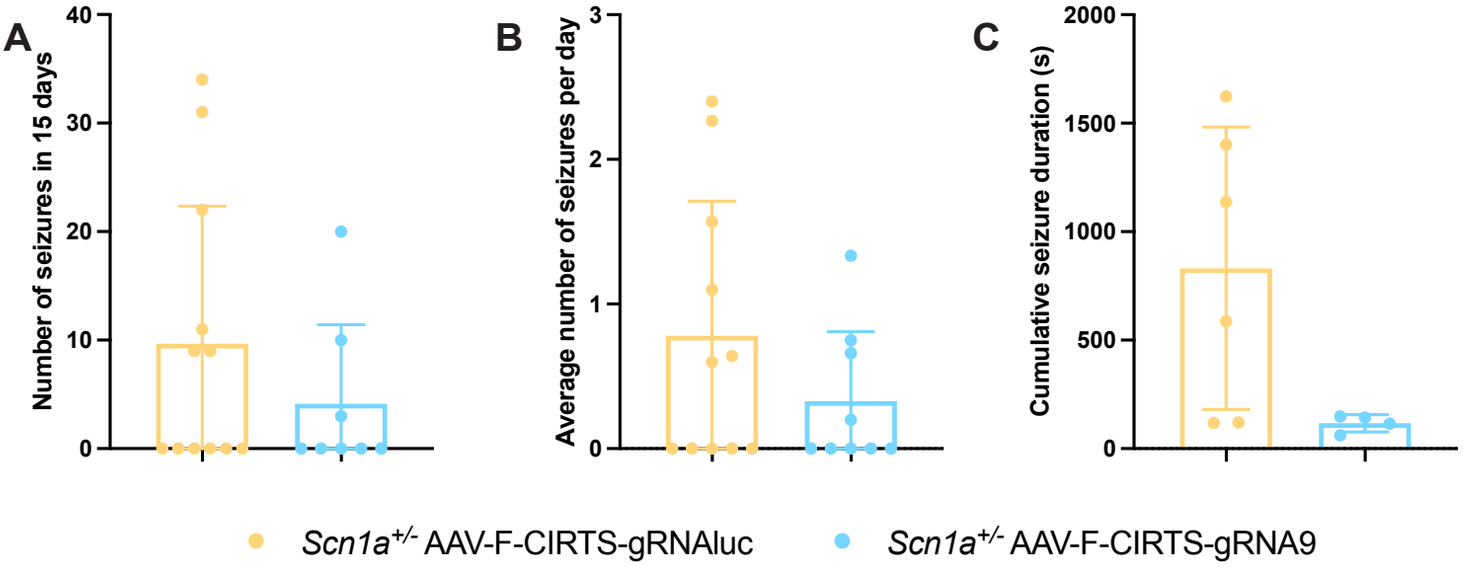

Supplementary Figure 11

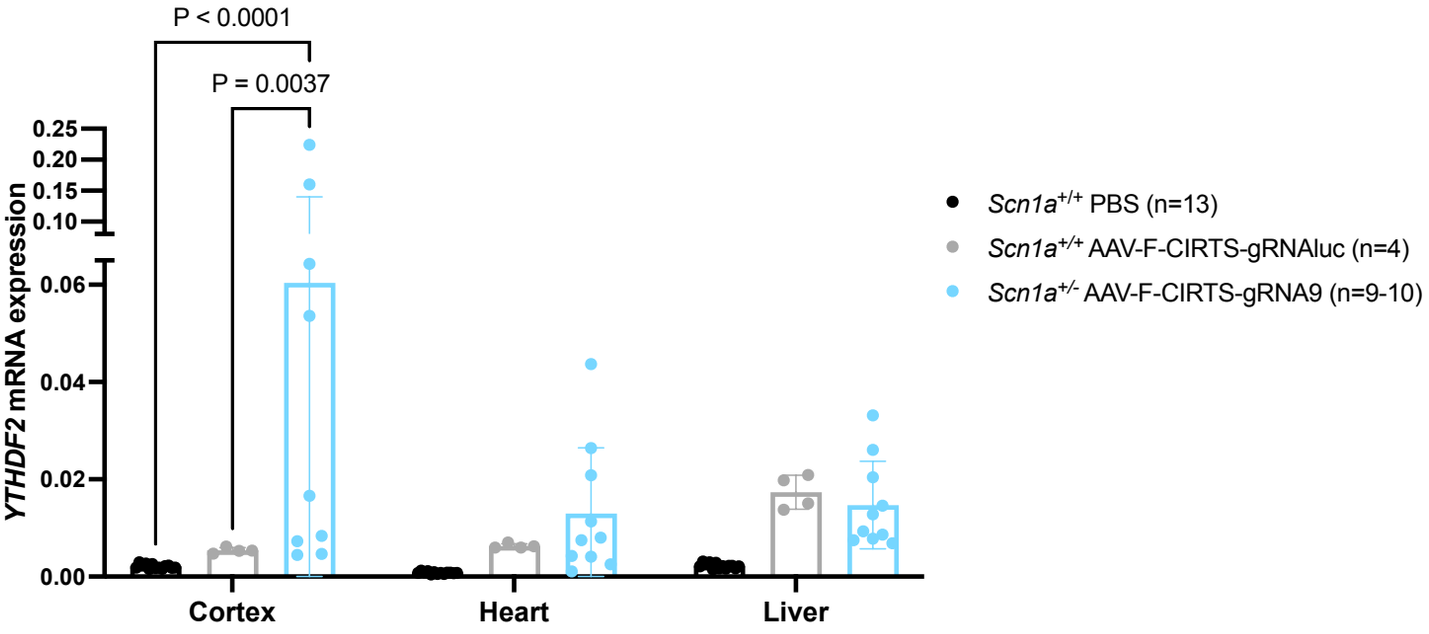
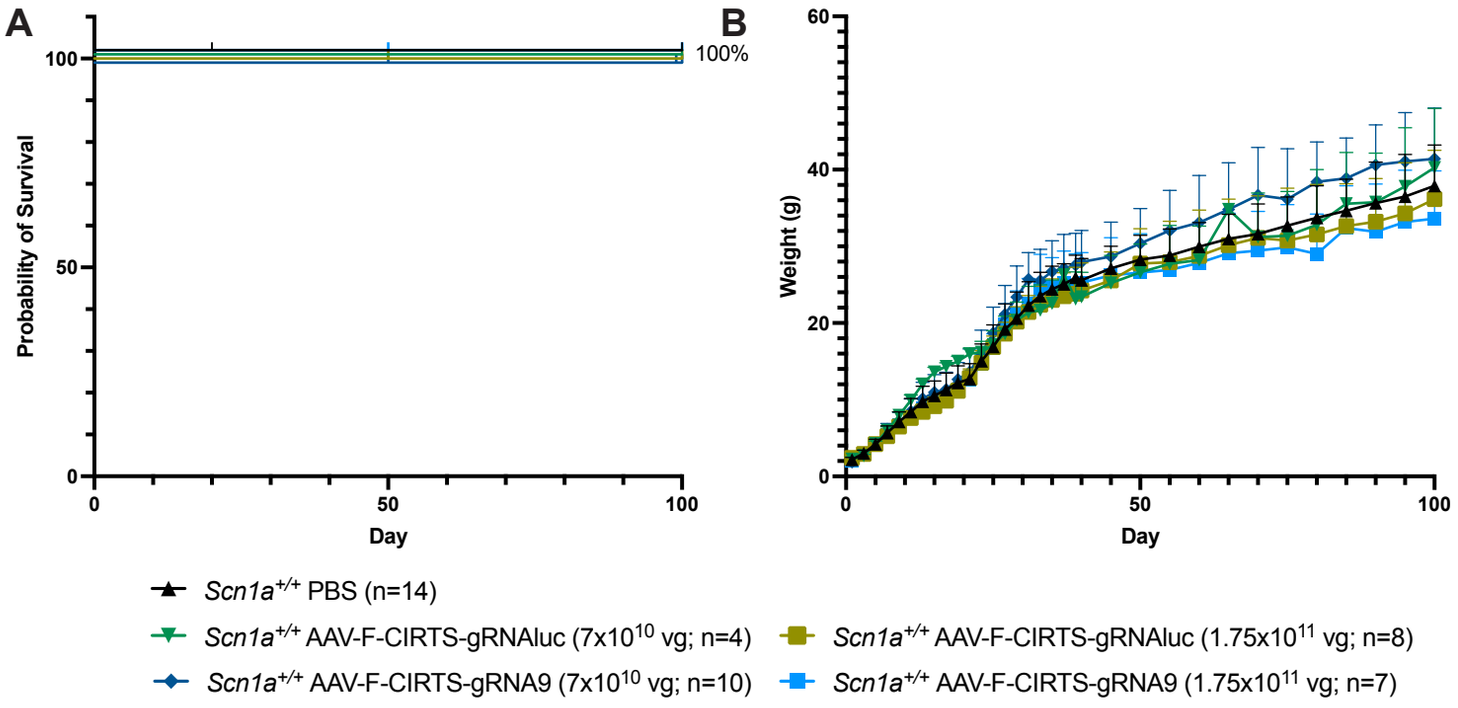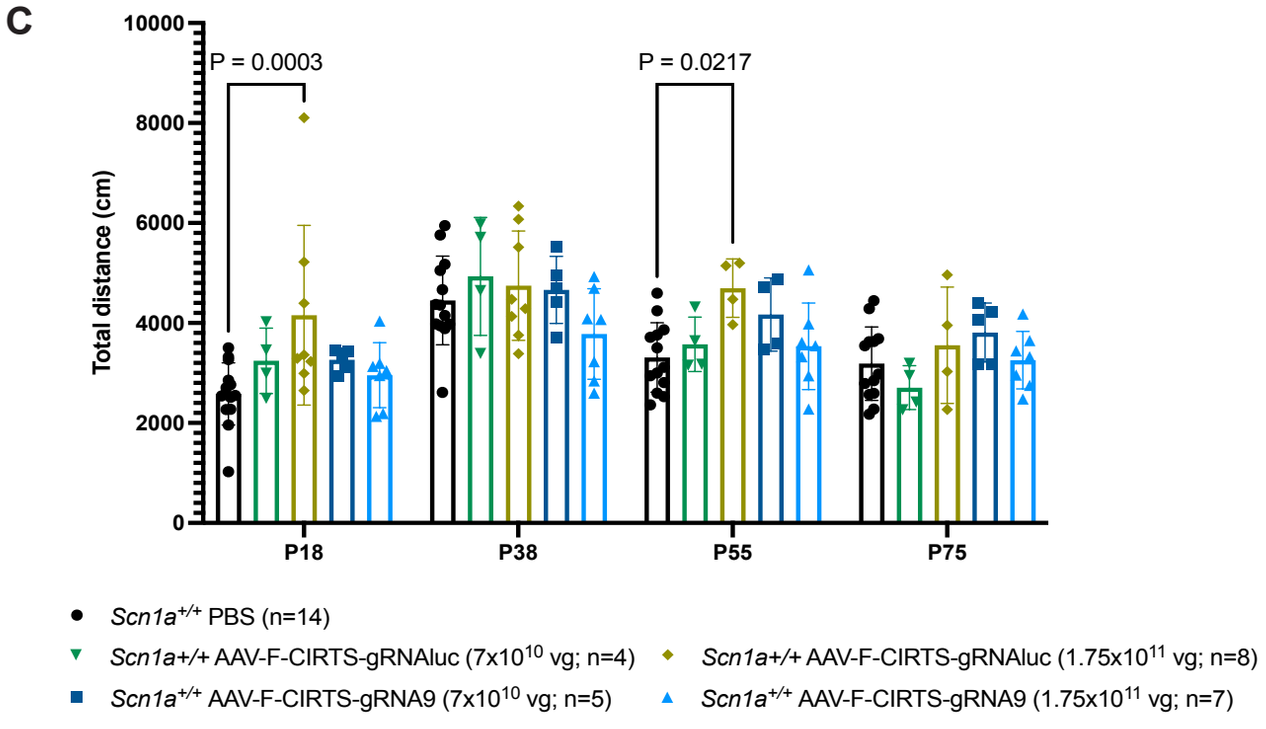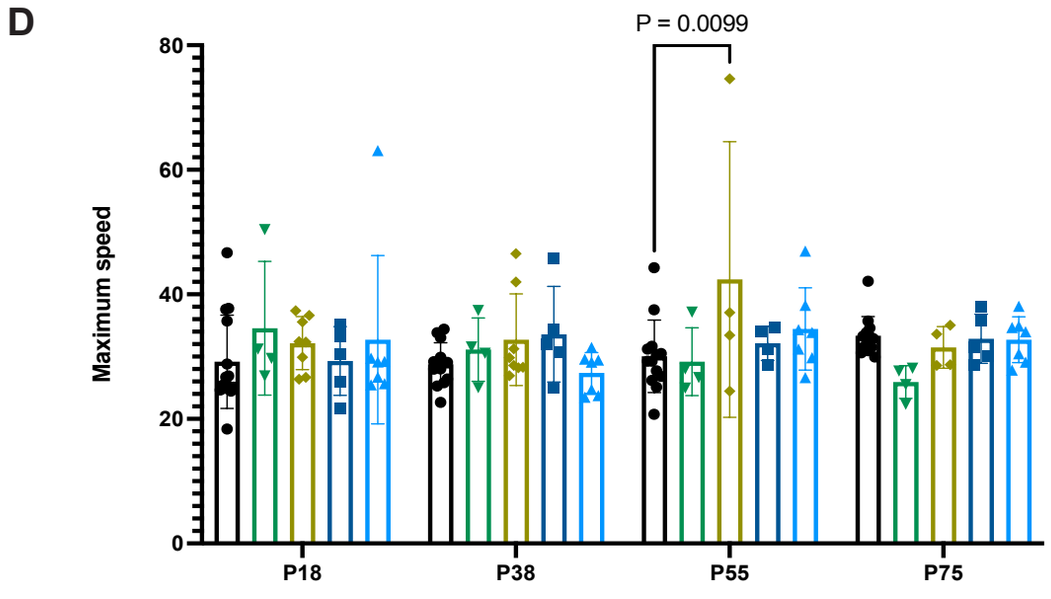
Supplementary Figure 12